



HAL
open science

The dust load and radiative impact associated with the June 2020 historical Saharan dust storm

Diana Francis, Narendra Nelli, Ricardo Fonseca, Michael Weston, Cyrille
Flamant, Charfeddine Cherif

► To cite this version:

Diana Francis, Narendra Nelli, Ricardo Fonseca, Michael Weston, Cyrille Flamant, et al.. The dust load and radiative impact associated with the June 2020 historical Saharan dust storm. *Atmospheric Environment*, 2022, 268, pp.118808. 10.1016/j.atmosenv.2021.118808 . insu-03402562v1

HAL Id: insu-03402562

<https://insu.hal.science/insu-03402562v1>

Submitted on 25 Oct 2021 (v1), last revised 31 Oct 2021 (v2)

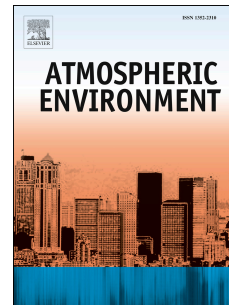
HAL is a multi-disciplinary open access archive for the deposit and dissemination of scientific research documents, whether they are published or not. The documents may come from teaching and research institutions in France or abroad, or from public or private research centers.

L'archive ouverte pluridisciplinaire **HAL**, est destinée au dépôt et à la diffusion de documents scientifiques de niveau recherche, publiés ou non, émanant des établissements d'enseignement et de recherche français ou étrangers, des laboratoires publics ou privés.



Distributed under a Creative Commons Attribution 4.0 International License

Journal Pre-proof



The dust load and radiative impact associated with the June 2020 historical Saharan dust storm

Diana Francis, Narendra Nelli, Ricardo Fonseca, Michael Weston, Cyrille Flamant, Charfeddine Cherif

PII: S1352-2310(21)00630-0

DOI: <https://doi.org/10.1016/j.atmosenv.2021.118808>

Reference: AEA 118808

To appear in: *Atmospheric Environment*

Received Date: 28 May 2021

Revised Date: 19 October 2021

Accepted Date: 20 October 2021

Please cite this article as: Francis, D., Nelli, N., Fonseca, R., Weston, M., Flamant, C., Cherif, C., The dust load and radiative impact associated with the June 2020 historical Saharan dust storm, *Atmospheric Environment* (2021), doi: <https://doi.org/10.1016/j.atmosenv.2021.118808>.

This is a PDF file of an article that has undergone enhancements after acceptance, such as the addition of a cover page and metadata, and formatting for readability, but it is not yet the definitive version of record. This version will undergo additional copyediting, typesetting and review before it is published in its final form, but we are providing this version to give early visibility of the article. Please note that, during the production process, errors may be discovered which could affect the content, and all legal disclaimers that apply to the journal pertain.

© 2021 Published by Elsevier Ltd.

The Dust Load and Radiative Impact associated with the June 2020 historical Saharan Dust Storm

Diana Francis^{1*}, Narendra Nelli¹, Ricardo Fonseca¹, Michael Weston¹, Cyrille Flamant², Charfeddine Cherif¹

¹ Environmental and Geophysical Sciences Lab, Khalifa University, P.O. Box 127788, Abu Dhabi, UAE.

² CNRS and UVSQ, LATMOS, Sorbonne Universités, 75005 Paris, France.

Corresponding Author: diana.francis@ku.ac.ae

Credit Author Statement:

Diana Francis: Conceptualization, Methodology, Investigation, supervision, Original draft preparation and Reviewing.

Narendra Nelli: Visualization, data curation and analysis.

Ricardo Fonseca: Formal analysis, Validation, Writing - Original draft preparation and Reviewing.

Michael Weston: Performance of WRF model simulations and analysis.

Cyrille Flamant: Analysis and validation.

Charfeddine Cherif: Software, Data curation.

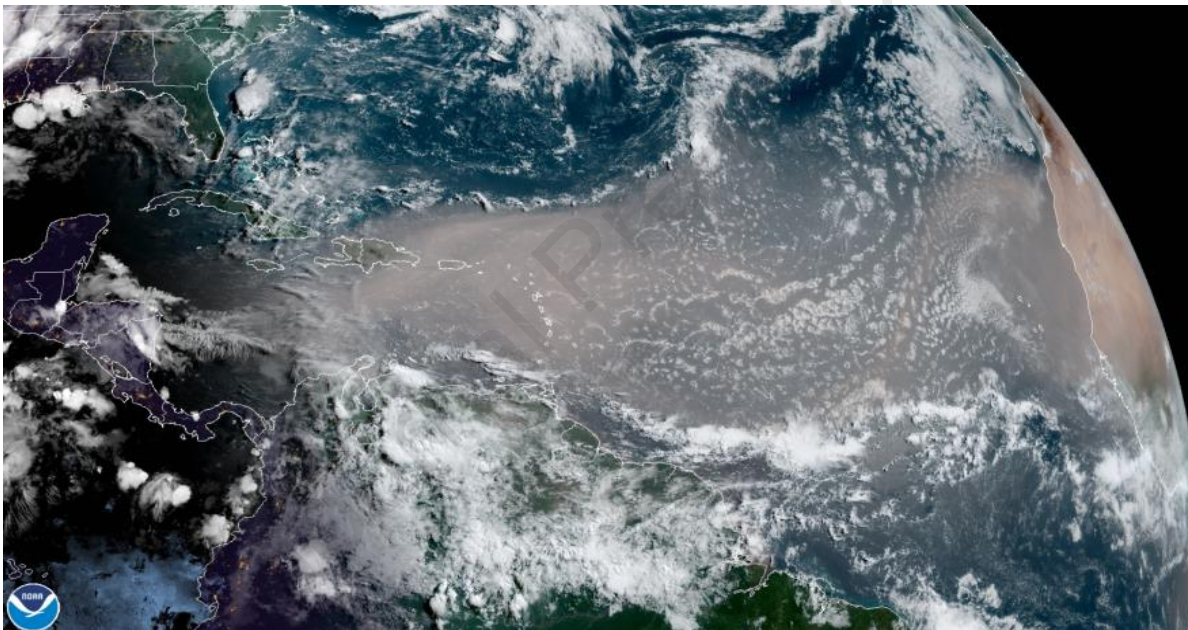
The Dust Load and Radiative Impact associated with the June 2020 historical Saharan Dust Storm

Diana Francis^{1*}, Narendra Nelli¹, Ricardo Fonseca¹, Michael Weston¹, Cyrille Flamant², Charfeddine Cherif¹

¹ Environmental and Geophysical Sciences Lab, Khalifa University, P.O. Box 127788, Abu Dhabi, UAE.

² CNRS and UVSQ, LATMOS, Sorbonne Universités, 75005 Paris, France.

Corresponding Author: diana.francis@ku.ac.ae



The Saharan dust storm in June 2020 over the Atlantic Ocean heading to the Caribbean.
Image Credit: NOAA.

Dust is an important component of the Earth's atmosphere, with a wide range of impacts ranging from human health to effects on the ocean and climate. In fact, airborne dust aerosols modify the energy budget of the Earth's surface by interacting with the solar radiation in different ways where they absorb in the ultraviolet and longwave and reflect in the shortwave. In June 2020, massive amounts of dust were lifted from the Sahara, the major dust source region in the world, and transported all the way into the Americas across the tropical Atlantic Ocean. During this event, large dust loads, in excess of 8 Tg, covered the tropical Atlantic Ocean and induced a radiative forcing at the surface. The energy budget of the atmosphere and the ocean surface was impacted during this event resulting in a sustained warming during night and a cooling during day. The resulting effect of dust during this event was an increase in the air temperature and the sea surface temperature associated with an increase in the longwave radiation especially during night due to the re-emission of radiation towards the surface by the dust clouds. This warming may have contributed to the very active tropical storms' season in summer 2020.

The Dust Load and Radiative Impact associated with the June 2020 historical Saharan Dust Storm

Diana Francis^{1*}, Narendra Nelli¹, Ricardo Fonseca¹, Michael Weston¹, Cyrille Flamant², Charfeddine Cherif¹

¹ Environmental and Geophysical Sciences Lab, Khalifa University, P.O. Box 127788, Abu Dhabi, UAE.

² CNRS and UVSQ, LATMOS, Sorbonne Universités, 75005 Paris, France.

Corresponding Author: diana.francis@ku.ac.ae

Highlights:

- June 2020 Saharan dust storm associated with highest-on-record aerosol optical depths;
- The estimated dust loads exceeded 8 Tg over the eastern tropical Atlantic;
- The dust event caused a net warming of the ocean surface by up to 1.1 K;
- Dust may have contributed to the extremely active 2020 Atlantic hurricane season.

Abstract

In June 2020, a major dust outbreak occurred in the Sahara that impacted the tropical Atlantic Ocean. In this study, the dust load and radiative forcing of the dust plumes on both the atmosphere and ocean surface is investigated by means of observations and modelling. We estimated dust loadings in excess of 8 Tg over the eastern tropical Atlantic, comparable to those observed over the desert during major Saharan dust storms. The dust induced an up to 1.1 K net warming of the ocean surface and a 1.8K warming of the air temperature (i.e., two to three times the respective climatological standard deviations), with a $+14 \text{ W m}^{-2}$ (~28% of the mean value) increase in the surface net radiation flux at night. As the dust plumes extended all the way to the Caribbean, it is possible that this historical dust event helped fuel the record-breaking 2020 Atlantic hurricane season.

Keywords: Dust aerosols, radiative forcing, Sahara, Tropical Atlantic, WRF-Chem.

33 1. Introduction

34 Aerosols have a profound impact on the surface and atmospheric energy budgets, owing to
35 their interaction with the radiation and cloud microphysics (e.g., Haywood and Boucher, 2000;
36 Satheesh and Moorthy, 2005). The most abundant aerosol type on Earth is mineral dust, with the
37 Sahara Desert its major source (Kok et al., 2021). Dust has an important impact on the climate
38 system (e.g., Choobari et al., 2014). For example, its accurate representation has been shown to
39 help in the simulation of the tropical/monsoon precipitation (e.g., Zhao et al., 2011; Balkanski et
40 al., 2021), hurricanes and tropical storms (e.g., Chen et al., 2017), local and regional weather
41 conditions (e.g., Spyrou et al., 2013; Weston et al., 2020; Francis et al., 2020a), and ocean
42 dynamics (e.g., Evan et al., 2012). Furthermore, mineral dust is known to strongly influence the
43 radiative budget due to its significant scattering, absorbing and re-emitting properties (Haywood
44 et al., 2005; Prakash et al., 2015; Di Bagio et al., 2017). By virtue of their distinctive optical
45 properties, mineral dust aerosols scatter and absorb shortwave (SW) and absorb and re-emit
46 longwave (LW) radiation (e.g., Sokolik et al., 2001; Dubovik et al., 2006), therefore modifying
47 the atmospheric thermodynamics and regional atmospheric circulations (e.g., Heald et al., 2014;
48 Francis et al., 2020a). Besides the aforementioned surface and atmospheric changes, dust carries
49 with it pollutants, some of which are toxic (e.g. pesticides and herbicides), and microorganisms
50 (e.g. fungi, viruses and bacteria) that can have harmful effects on the fauna and flora (e.g. Griffin
51 et al., 2002). In fact, Azua-Bustos et al. (2019) reported that a number of viable bacteria and fungi
52 can traverse the Atacama Desert unscathed using wind-transported dust, stressing how they can
53 propagate far away from the source region and affect different ecosystems. Dust outbreaks are
54 therefore linked to human health and air quality impacts. When inhaled, the fine dust particles can
55 penetrate deep into the lungs, and the smallest ones even into the alveoli, increasing the risk of
56 cardiopulmonary diseases and leading to premature mortality (Ginnadaki et al., 2014). In addition,
57 the combination of wind and dust reduces visibility, having a pronounced impact on day-to-day
58 activities such as transportation and agriculture (e.g. Al-Hemoud et al., 2017).

59
60 By absorbing and scattering solar radiation, dust aerosols reduce the amount of energy reaching
61 the surface (e.g., Kosmopoulos et al., 2017; Jia et al., 2018), which can lead to reduced surface
62 heating and thus latent and sensible heat fluxes (Wang et al., 2004; Prakash et al., 2015; Kaskaoutis
63 et al., 2019). At the same time, dust absorption of both LW and SW radiation can contribute to
64 localized heating by directly warming the dust-laden atmospheric layer (e.g., Weston et al., 2020;
65 Francis et al., 2020a), and enhance the greenhouse effect by re-emitting LW radiation towards the
66 surface (Heinold et al., 2008; Francis et al., 2020a). In all cases, the intensity of the radiative impact
67 of dust in both SW and LW depends strongly on the location of the dust layer in altitude (e.g.,
68 Saleeby et al., 2019), and whether it's over water, vegetated areas or desert lands (e.g., Wang et
69 al., 2013). Over the last few decades, dust aerosols have been thought to induce a net cooling at
70 the surface and contribute to the decrease in tropical storm activity over the tropical Atlantic (e.g.,
71 Evan et al., 2006). However, recent studies found that the warming effect of dust aerosols has been
72 previously underpredicted due to the underestimation of the amount of large particles in the

73 atmosphere (e.g., Adebisi and Kok, 2020), and the misrepresentation of their effect in the LW
74 radiation (Francis et al., 2020a).

75
76 One of the most daunting challenges in our understanding of dust and its impacts on the climate
77 system is the quantification of the dust net radiative effect (DRE; Sokolik et al., 2001) accounting
78 for both SW and LW interactions. This remains challenging mainly because of the lack of
79 observations at large scale and of a full understanding of the complexity of the processes involved
80 as well as the feedback among them. In addition, the DRE is highly dependent on dust properties,
81 such as size, shape and composition (Wang et al., 2006; Rontu et al., 2020; Ito et al., 2021). In this
82 case, the use of modelling approaches is common where the DRE can be estimated using the
83 observed dust properties and a radiative transfer model, or through coupled atmospheric-chemistry
84 models such as the Weather Research and Forecasting - Chemistry (WRF-Chem; Grell et al., 2005)
85 model, which is the case in this study. WRF-CHEM has been found to exhibit reasonable skill in
86 simulating dust storms and the direct effect of dust aerosols (e.g., Liu et al., 2016; Singh et al.,
87 2021), including over North Africa (e.g., Teixeira et al., 2016; Flaounas et al., 2017).

88
89 Haywood et al. (2003) and Highwood et al. (2003) examined the DRE of a mineral dust storm
90 off the coast of Africa in the year 2000 during the Saharan Dust Experiment (SHADE)
91 measurement campaign (Tanre et al., 2003). They measured a peak SW DRE of up to -130 W m^{-2}
92 (Haywood et al., 2003) and a corresponding LW DRE of around $+7 \text{ W m}^{-2}$ at the surface (Highwood
93 et al., 2003). This indicates that, for clear sky conditions over the ocean, the reduction in SW
94 radiation flux exceeds in magnitude the increase in LW flux, in line with the findings of other
95 studies (e.g., Slingo et al., 2006). For the same field campaign, Myhre et al. (2003) reported
96 Aerosol Optical Depths (AODs), an indication of the attenuation of the incoming SW radiation
97 due to the presence of aerosols, in excess of 1.5 at the offshore Cape Verde Islands on 26
98 September, when the modelled net radiative impact of the mineral dust over the eastern tropical
99 Atlantic peaked at around -110 W m^{-2} . Even far away from the source region Saharan dust can have
100 a pronounced radiative impact. For example, Gutleben et al. (2020), and in the vicinity of Barbados
101 in the Caribbean, estimated maximum SW radiative effects of -40 W m^{-2} (at the surface) and -25
102 W m^{-2} (at the TOA) for a dust event in August 2016, when the AOD exceeded 0.3. A comparable
103 variation of the radiation fluxes, but for the daily-mean values, was noted by Kaskaoutis et al.
104 (2019) for a dust storm in Greece in March 2018, when AODs higher than 4 were observed.
105 Dust storms have repeatedly impacted the entire Mediterranean Basin, spanning from the Iberian
106 Peninsula on the western side (e.g. Anton et al., 2014) to Cyprus on the eastern side (e.g. Uzan et
107 al., 2018). For a dust storm in southeastern Spain on 06 September 2007, Anton et al. (2014) noted
108 that, for a one unit increase in the AOD at 675 nm, the SW irradiance at the surface decreased by
109 187 W m^{-2} and the LW irradiance increased by 20 W m^{-2} (the observed AOD was in the range 0.8
110 to 1.5). Therefore, as the dust loading goes up, the offset of the decrease in the SW irradiance by
111 the increase in the LW irradiance becomes smaller, dropping from 40% for an AOD of 0.8 to 20%
112 for an AOD of 1.5. A very severe dust storm affected the eastern Mediterranean in September

113 2015, with AODs at 550 nm exceeding 5 in Cyprus (Solomos et al., 2017), and extended into the
114 Middle East (Francis et al., 2019). Surface radiation measurements in northern Israel revealed a
115 roughly 600 W m^{-2} drop in the global solar radiation in association with the event, with dust layers
116 up to 5 km (Uzan et al., 2018).

117
118 Saidou Chaibou et al. (2020) investigated the DRE over western Africa and its impact on the
119 surface and TOA energy budget during summer 2006. The DRE is estimated by taking the
120 difference between a simulation in which the dust radiative effects are considered and one where
121 the radiative impacts are not activated. The DRE at the TOA is positive over the Sahara Desert
122 and negative over the Gulf of Guinea and vegetated areas, with a mean value of $+9 \text{ W m}^{-2}$. On the
123 other hand, the mean DRE at the surface is -13 W m^{-2} , reflecting the cooling by dust aerosols. In
124 addition to its impact on the SW and LW fluxes, dust aerosols also affect the other terms of the
125 surface energy budget: e.g. the sensible heat flux (SHF) is cut by up to 24 W m^{-2} , owing to a colder
126 surface by up to 2°C , while the latent heat flux (LHF) increases up to 12 W m^{-2} over the desert
127 (evaporation) and is lower by up to 24 W m^{-2} over the vegetated regions further south. What is
128 more, the DRE also exhibits a clear diurnal cycle, as the SW radiation flux is only non-zero during
129 daytime meaning that, at night, the LW radiation flux will balance the heat fluxes and ground heat
130 flux (Nelli et al., 2020).

131
132 A recent record-breaking Saharan dust storm took place in mid-June 2020. As detailed in
133 Francis et al. (2020b), this event was triggered by a pressure dipole over northwestern Africa, with
134 a ridge, associated with a circum-global wavetrain, just to the west of the Saharan heat low. This
135 dipole led to persistent northeasterly winds and continuous dust emissions over a 4-day period.
136 While the mechanisms behind the observed event are discussed in detail in Francis et al. (2020b),
137 no attempt has been made to quantify the lifted dust and its radiative impact. This will be addressed
138 in the present paper. The goal of this study is twofold: (i) estimate the amount of dust aerosols
139 emitted during the event and compare it to dust emissions available in the literature; (ii) estimate
140 the DRE over the Atlantic Ocean during the event, and speculate on its implications in particular
141 on the tropical cyclone activity, as the eastern tropical Atlantic around the Cape Verde islands, the
142 target region in this study, is a primary breeding area for Atlantic hurricanes (e.g. Haggard, 1958).
143 The findings of this work will help to better understand the effects of dust on the climate system,
144 in particular as major dust storms, such as the June 2020 Saharan dust storm, may become more
145 frequent in a warming climate (e.g., Bellouin et al., 2020).

146
147 This paper is structured as follows. In section 2, a summary of the observational and modelling
148 products used in this study is given. The experimental set up of WRF-CHEM is also described.
149 The dust load and DRE estimates and their implications are discussed in section 3, while in section
150 4 the main findings are outlined.

151

152 2. Data and methods

153 2.1 Observational & Reanalysis Datasets

154 Five observational datasets are used in this work, four of which are satellite-derived products
155 while the last one comprises ground-based measurements.

- 156 ➤ Red-Green-Blue (RGB) satellite images from the Spinning Enhanced Visible and Infrared
157 Imager (SEVIRI; Schmetz et al., 2002) instrument on board the Meteosat Second
158 Generation Spacecraft, from 17 to 24 June 2020 (0.05°; 15-min). These images are
159 constructed using the brightness temperatures measured at the 8.7, 10.8, and 12 μm infrared
160 channels (Martinez et al., 2009);
- 161 ➤ AOD estimates from the (i) Visible Infrared Imaging Radiometer Suite (VIIRS; Miller et
162 al., 2013) instrument onboard the Suomi National Polar-orbiting Partnership satellite (6
163 km; hourly), and (ii) the Moderate Resolution Imaging Spectroradiometer (MODIS;
164 Kaufman et al. 1997) instrument on board the Terra and Aqua satellites (1 km; daily). The
165 MODIS products MOD04_L2 and MYD04_L2, algorithm version 6 and level 2 data, are
166 used (Levy and Hsu, 2015a,b). ;
- 167 ➤ Clouds and the Earth's Radiant Energy System (CERES; Doelling et al., 2013, 2016; 1°
168 and hourly) surface SW, LW and net radiation fluxes derived from satellite estimates;
- 169 ➤ The Group of High-Resolution Sea Surface Temperature (GHRSSST; Martin et al., 2012)
170 Level 4 data provides foundation SSTs from a combination of different satellite
171 measurements (0.01°; daily);
- 172 ➤ The Aerosol Robotic Network (AERONET; Holben et al., 1998) is a network of ground-
173 based sun photometers that provide 15-min estimates of the AOD at wavelengths in the
174 range 340 to 1640 nm.

175
176 Regarding the satellite-derived AOD estimates, it is important to note that, while MODIS' AOD
177 is closer to that estimated using ground-based assets when compared to that given by VIIRS, in
178 particular in desert regions, it has more gaps than the latter (Wang et al. 2017, 2020), and hence
179 the two are used in this study. What is more, the agreement between MODIS AOD and that given
180 AERONET's sun photometers is not always optimal. As noted e.g. by Levy et al. (2005), over
181 land, and in particular in the blue wavelength, MODIS AOD tends to be higher in cleaner
182 environments and lower in dustier environments when compared with ground-based estimates.
183 This likely arises because of an incorrect setting of the surface albedo in the lookup tables. Other
184 sources of error include sub-pixel cloud, snow/ice and water contamination (Chu et al., 2002), as
185 well as varying aerosol properties such as shape (Remer et al., 2005).

186
187 In addition to the datasets listed above, ERA-5 (Hersbach et al., 2020) and the Modern-Era
188 Retrospective analysis for Research and Applications version 2 (MERRA-2; Gelaro et al., 2017)
189 reanalysis data are considered. ERA-5 data is available at 0.25° x 0.25° on an hourly basis from
190 1979 to present, and has the highest spatial and temporal resolution of any publicly available

191 reanalysis dataset at the time of writing of the paper. MERRA-2 is unique in the sense that it
192 represents aerosols and their interactions with the climate system, allowing for explicit predictions
193 of the AOD and column dust mass loading, which are available at $0.625^\circ \times 0.5^\circ$ and 1-hour
194 resolution.
195

196 **2.2 WRF-CHEM Simulations**

197 Dust emissions and transport were simulated using WRF-Chem v3.9.1.1 (Grell et al., 2005,
198 Skamarock et al., 2008). A single domain, which covered most of North Africa and adjacent
199 Atlantic Ocean (38.58°W - 41.58°E ; 1.35°N - 37.63°N) at 12 km resolution was used, with 45
200 vertical levels. Simulations were forced with the 6-hourly National Centers for Environmental
201 Prediction (NCEP) Global Forecast System (GFS; NCEP, 2015) $0.25^\circ \times 0.25^\circ$ data. A summary
202 of the model configuration is presented in Table 1.
203

204 In the model simulations, aerosol-radiation feedbacks are accounted for, while aerosol-cloud
205 interactions (i.e. aerosol indirect effects) are not activated. What is more, WRF-Chem is run with
206 dust emissions only, the gas-phase chemistry is not considered. In order to assess the impact of
207 dust aerosols on the radiation budget and atmospheric flow, similar simulations were run without
208 dust, with all other settings remaining unchanged. These two sets of model runs are labelled as
209 “WRF Dust” and “WRF No Dust” throughout the manuscript.
210

211 Dust emissions in the model are controlled by the Air Force Weather Agency (AFWA) dust
212 scheme described by Legrand et al. (2018). This scheme uses the erodibility map developed by
213 Ginoux et al (2001) to represent the source strength of emissions. A feature of this scheme is that
214 it accounts for dust emission by three mechanisms: aerodynamic lift, saltation bombardment and
215 particle disaggregation (Legrand et al., 2018). Aerodynamic lift is when particles become airborne
216 due to wind shear. A characteristic of this process is that small particles (diameter $< 10\mu\text{m}$) remain
217 on the surface due to forces of adhesion and cohesion, while larger particles (10 - $250\mu\text{m}$) become
218 lofted (e.g. Colarco et al., 2003). The larger particles then return to the surface (saltation
219 bombardment), where the impact causes the smaller particles to overcome the adhesion and
220 become dislodged and lofted. Dust is emitted into the lowest model level and transported from
221 there in 5 size-bins that range from 0.2 to $20\mu\text{m}$. Land cover classes are taken from the United
222 States Geological Survey (USGS) global database (Loveland et al., 2000, Sertel et al., 2010). The
223 default soil texture in WRF is from the State Soil Geographic (STATSGO)/Food and Agriculture
224 Organization (FAO) soil database (Sanchez et al., 2009; Dy and Fung, 2016). At the lower
225 boundary over the ocean, a simple prognostic scheme is employed for the sea surface skin
226 temperature (SSKT), which is essentially controlled by the SSTs from the GFS forcing data. This
227 parameterization scheme, based on Zeng and Beljaars (2005), accounts for the effects of the
228 radiative and heat fluxes, as well as molecular diffusion and turbulent mixing, and allows the
229 model to simulate the diurnal variability in the SSKT and its feedback to the atmosphere.

230

Parameterization	Scheme
Radiation SW	Rapid Radiative Transfer Model for GCMs (Iacono et al., 2008)
Radiation LW	Rapid Radiative Transfer Model for GCMs (Iacono et al., 2008)
Boundary Layer	Yonsei University Planetary Boundary Layer (Hong et al., 2006)
Cumulus	Grell 3 (Grell and Dvnyi, 2002)
Microphysics	Lin (Lin et al., 1983)
Land Surface Model	NOAH (Tewari et al., 2004)
Surface Layer	Revised MM5 (Jimenez et al., 2012)
Chemistry	WRF Dust Simulation: Goddard Chemistry Aerosol Radiation and Transport simple/no ozone (gas-phase chemistry not activated) WRF No Dust Simulation: Chemistry module switched off
Dust option	Air Force Weather Agency dust scheme (Legrand et al., 2018)
Aerosol- radiation feedback	Active
Aerosol-cloud feedback	Inactive
Aerosol Optics	Volume approximation

231

232

Table 1. WRF-Chem physics and chemistry parameterization

233

234 As the dust event lasted for more than 5 days it was decided to break up the simulations into
 235 shorter periods, with the model initialized at 00 UTC every 48 h from 12 to 22 June 2020. The
 236 chemistry variables, which is only dust in this case, from the previous model run are used as input
 237 at the start of the subsequent simulation. For each simulation, the first 12 h are discarded as spin
 238 up while the following 36 h (i.e. forecast hours +13 to +48) are retained for analyses.

239

240 The aerosol optical properties, such as the extinction coefficient, at different wavelengths in
 241 the SW and LW portions of the electromagnetic spectrum, including at 550 nm, are calculated for
 242 each model level (Barnard et al., 2010). The AOD is calculated in post-processing by integrating
 243 the extinction coefficient, which is explicitly predicted by WRF-Chem for each model layer,
 244 over all model layers. Hereafter, the 550 nm AOD will be referred to just as AOD for simplicity.

245 **3. Results**246 **3.1 Estimation of Dust Load**

247 As detailed in Francis et al. (2020b), the June 2020 Sahara dust storm was of historic
 248 proportions. Not only were record amounts of dust present in the atmosphere (as evidenced e.g. by
 249 the highest ever AOD recorded at an AERONET station in Cape Verde), but the associated dust
 250 plume reached all the way to North America. The extreme nature of this event can be seen in Fig.
 251 1, which shows RGB composites from SEVIRI from 17 to 24 June during nighttime (01 UTC) and
 252 daytime (13 UTC). The dust emissions over the Sahara and the westward propagation of the dust
 253 plume (pink shading), aided by an anomalously strong African Easterly Jet, can be clearly seen.
 254

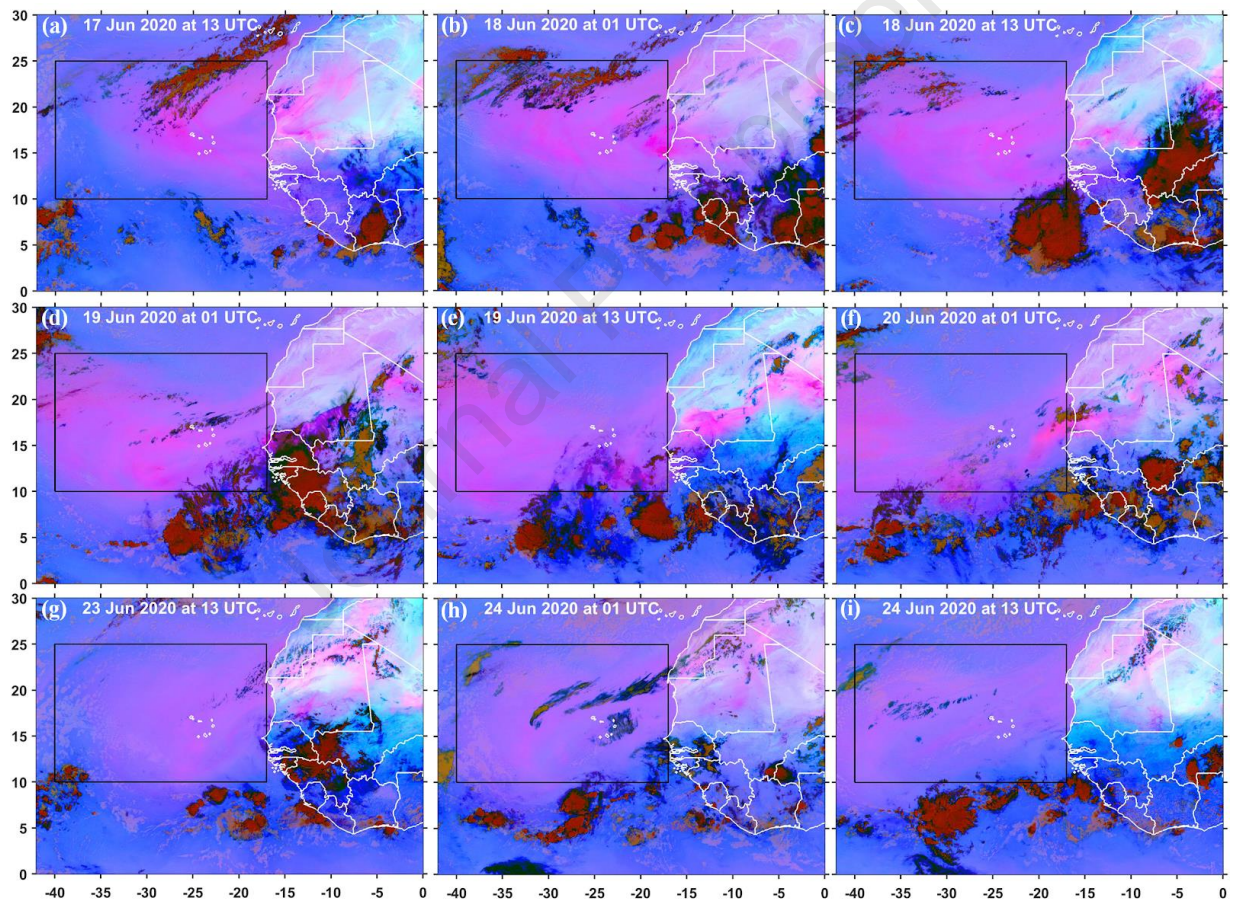


Figure 1. SEVIRI dust RGB snapshots from 17 to 24 June 2020 at 01 UTC (nighttime) and 13 UTC (daytime). In all panels, dust is given in magenta or pink; thick high-level clouds are shaded in orange or brown; thin high-level clouds appear very dark (nearly black); sandy regions are highlighted in white. Dry land is shaded in pale blue during daytime and pale green at night. The region $40^{\circ}\text{W}-17^{\circ}\text{W}$ & $10^{\circ}\text{N}-25^{\circ}\text{N}$ (used for averaging in subsequent figures), which encompasses the bulk of the dust plume at the beginning of the episode, is denoted by a black rectangle.

255

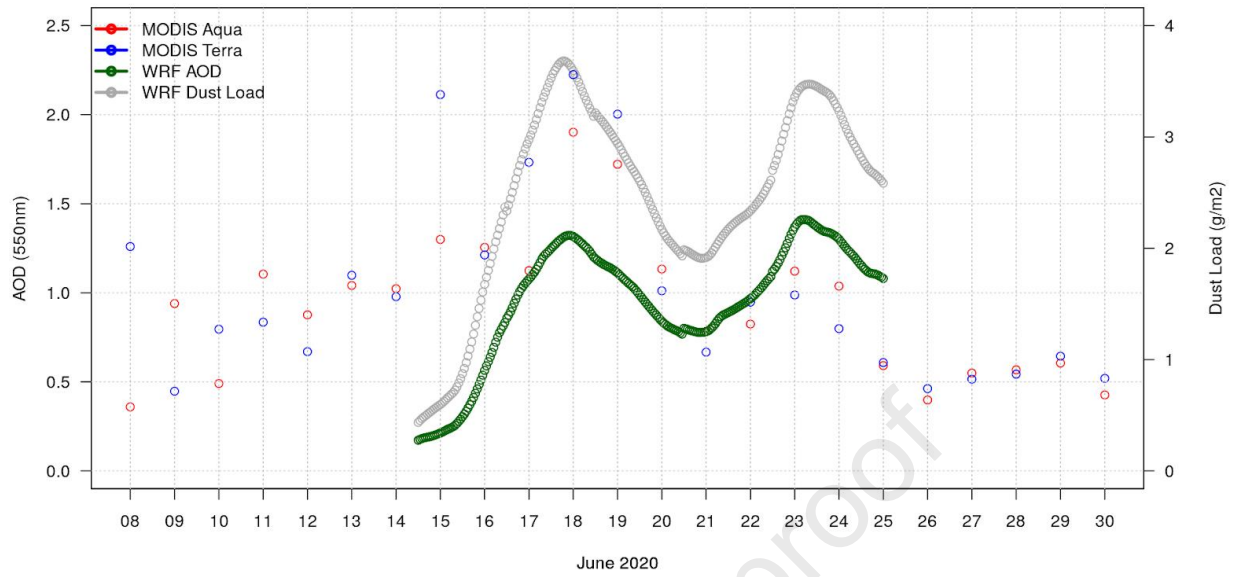
256 In order to quantify the amount of atmospheric dust, Figure 2 shows WRF and MERRA2-
 257 predicted and satellite-derived AOD, as well as modelled column dust mass on 18 June 2020. As

258 seen in Fig. 1, on this day a dust plume was located over the eastern tropical Atlantic around Cape
259 Verde. AOD estimates exceeded ~ 2 from MODIS (Fig. 2a) and were as high as ~ 5 from VIIRS
260 (Fig. 2b). Such high values of AOD are not unheard of (e.g. Solomos et al. (2018) and Kaskaoutis
261 et al. (2019) estimated AODs as high as ~ 6 during dust storms over the eastern Mediterranean),
262 but have not been observed before in the eastern tropical Atlantic (at least in the Cape Verde
263 Islands), as noted by Francis et al. (2020b). Having said that, it is perfectly possible that, in
264 particularly dusty conditions, such as during haboobs when the Sun can be completely obscured,
265 higher values of AOD have been observed. However, the retrieval algorithm likely flagged the
266 correspondent pixels as cloudy, meaning that such the AOD values are not reported in the
267 literature.

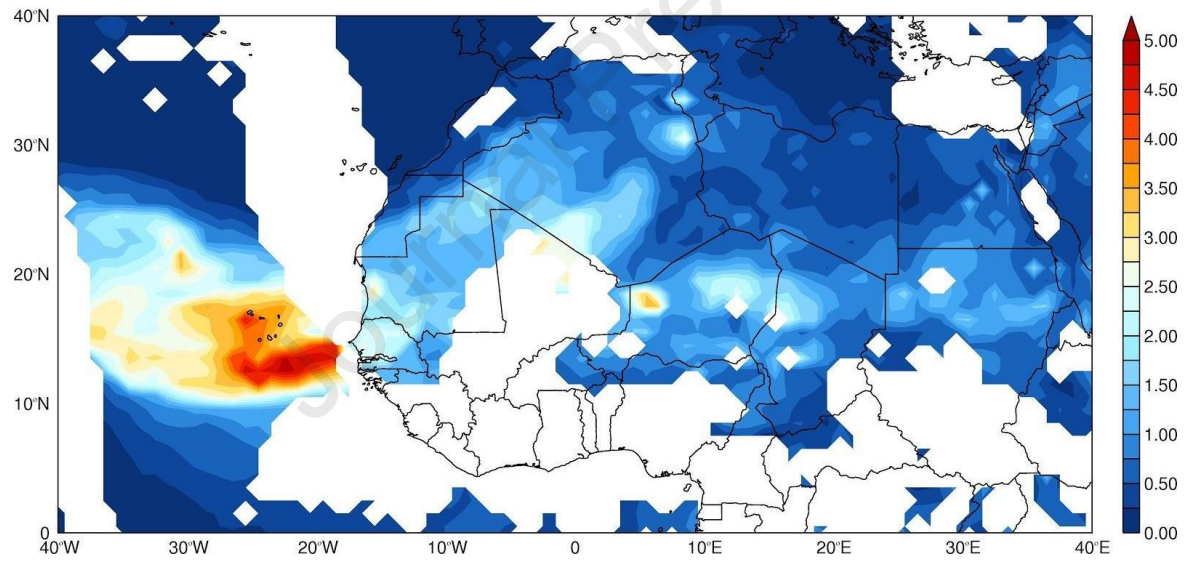
268
269 A comparison between the AOD from VIIRS (Fig. 2b) and that of MERRA-2 (Fig. 2d)
270 indicates a similar spatial pattern, even though MERRA-2 underestimates its magnitude. As noted
271 by Buchard et al. (2017), the assimilation of space-based observations of aerosols in the reanalysis
272 data does not correct for all the AOD biases, which are caused e.g. by missing emissions and/or
273 deficiencies in the parameterization schemes. The reanalysis data predicts more than 6 g m^{-2} of dust
274 over the tropical eastern Atlantic, with a maximum in the surface dust mass concentration of ~ 1200
275 $\mu\text{g m}^{-3}$. A comparison with other major dust storms revealed that this last figure is roughly (i) 30
276 times larger than that measured in Puerto Rico during the Sahara dust storm of March 2004
277 (Rodriguez-Cotto et al., 2013); (ii) four times higher than that observed in the Middle East during
278 six frontal dust storms in 2016-2018 (Hamzeh et al., 2021); (iii) up to 10 times larger than that
279 measured during a major dust storm in East Asia in April 2001 (Manktelow et al., 2010); and (iv)
280 comparable to the amount of dust emitted during major dust storms in the eastern Mediterranean,
281 where several studies reported surface dust concentrations of up to $6000 \mu\text{g m}^{-3}$ (Albert and Ganor,
282 2001; Saeed et al., 2014; Solomos et al., 2018; Kaskaoutis et al., 2019).

283

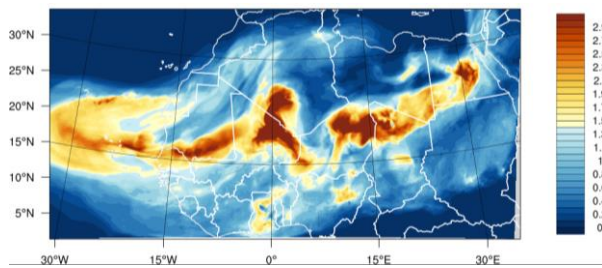
(a)



(b)

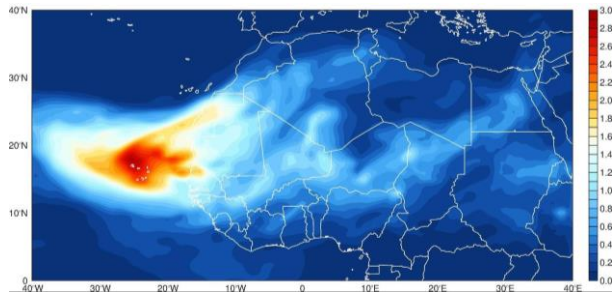


(c)



(e)

(d)



(f)

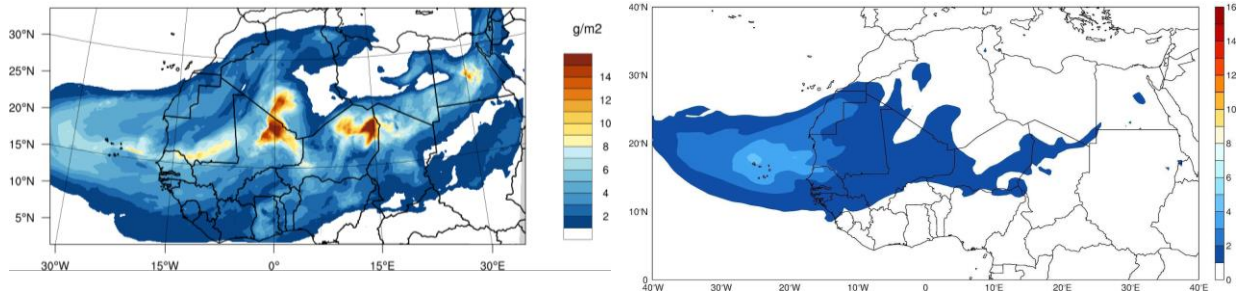


Figure 2 (a) WRF AOD (green circles, left axis) and dust load (grey circles, right axis; g m^{-2}) and MODIS AOD (blue and red circles; left axis), averaged over the eastern tropical Atlantic Ocean ($38^{\circ}\text{W}-17^{\circ}\text{W}$ & $10^{\circ}\text{N}-25^{\circ}\text{N}$), from 08 to 30 June 2020. Spatial distribution of the AOD over the study region on 18 June 2020 from (b) VIIRS satellite (daily maximum; the white shading denotes gaps in the data coverage), (c) WRF and (d) MERRA-2 at 00 UTC. (e) and (f) are as (c) and (d) but for the total column dust mass (g m^{-2}).

284

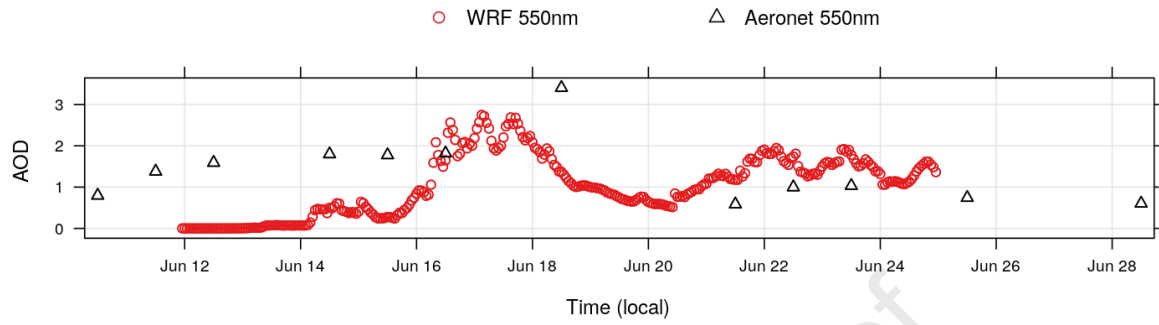
285 When integrated over the eastern tropical Atlantic ($40^{\circ}\text{W}-17^{\circ}\text{W}$ & $10^{\circ}\text{N}-25^{\circ}\text{N}$; black rectangle
 286 in Fig. 1), where the bulk of the dust plume is located, following Todd et al. (2008), the total dust
 287 loading is about 7.9 Tg, which is roughly comparable to that estimated over land during other major
 288 dust storms (Bou Karam et al. 2009, 2010, 2014; Francis et al., 2020a).

289

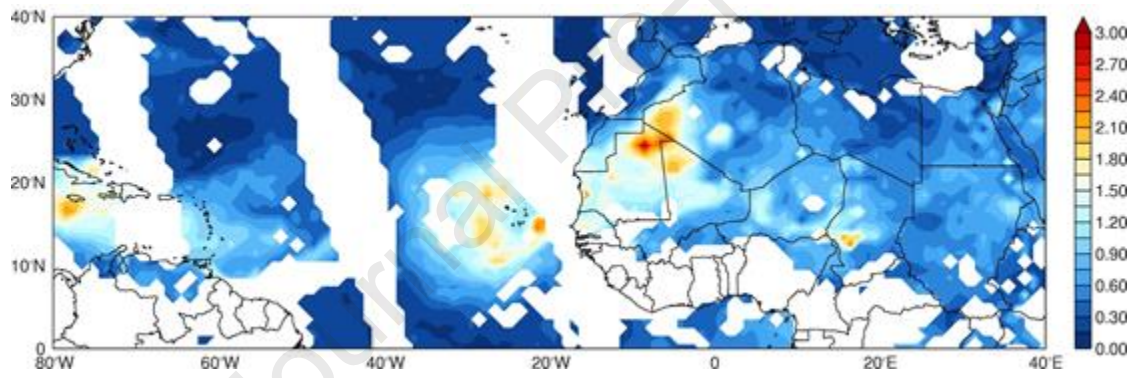
290 WRF underestimates the observed AOD over the eastern tropical Atlantic on 18 June, on
 291 average slightly more than MERRA-2: as seen in Fig. 2a, the WRF-predicted AOD is roughly 0.5-
 292 1 lower than that estimated from MODIS and AERONET, respectively. The fact that the
 293 atmosphere is less dusty in WRF may be due to (i) uncertainties in the dust parameterization
 294 schemes (e.g., Flaounas et al., 2017; Eltahan et al., 2018), which is also the case for MERRA-2;
 295 an incorrect representation of the (ii) large-scale circulation (e.g., Kabatas et al., 2018), and (iii)
 296 surface properties such as the erodibility factor (e.g., Su et al., 2015). The spatial pattern of the
 297 AOD in WRF (Fig. 2c) is also different to that of VIIRS (Fig. 2b) and MERRA-2 (Fig. 2d), with
 298 the dust being more concentrated over the desert. A possible reason for this is the lack of data
 299 assimilation in WRF, which is employed in the reanalysis dataset. However, the “tongue” of higher
 300 amounts of dust over northern Mali, and from Niger and northern Chad to central Egypt in WRF
 301 is also present in MERRA-2 and VIIRS. In particular over land, WRF predicts higher AODs than
 302 MERRA-2 (Fig. 2c-d), which is also reflected in the larger dust masses (Fig. 2e-f). However, over
 303 the eastern tropical Atlantic, the two are broadly in agreement. On 23 June (Fig. 3), the day of the
 304 second AOD peak, the WRF and observed AODs are more in line with each other (cf. Fig. 2a and
 305 Fig. 3a), with the spatial pattern of the AOD and dust loading also being generally similar between
 306 WRF and MERRA-2 (Fig. 3c-f), the latter in close agreement with the VIIRS estimates (Fig. 3b).
 307 As on 18 June, WRF predicts substantially higher amounts of dust over northwestern Africa
 308 compared to MERRA-2, with AODs roughly $\sim 1-2$ index units higher and a dust mass typically
 309 $\sim 3-5 \text{ g m}^{-2}$ larger than that in the reanalysis dataset. Despite this, over the eastern tropical Atlantic,
 310 the two continue to be closer to each other (Fig. 3c-f).

311

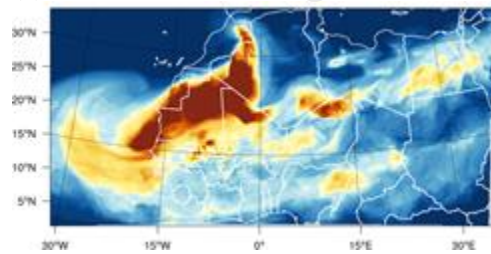
(a)



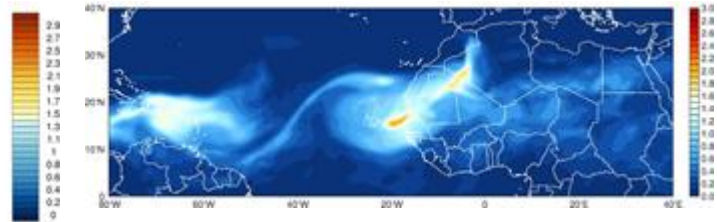
(b)



(c)



(d)



(e)

(f)

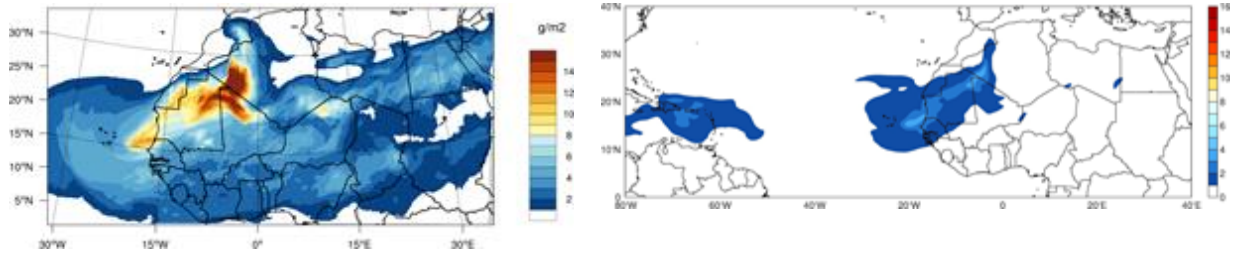
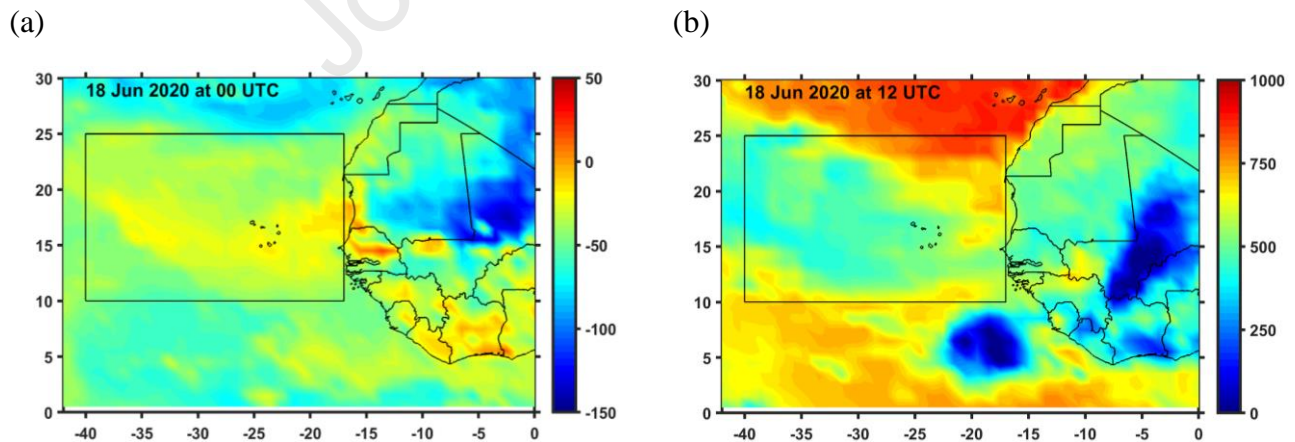


Figure 3 As Figure 2 but on 23 June 2020. In (a), the WRF and observed AOD at 550 nm from 10 to 29 June 2020 are plotted at the location of the AERONET station in Cape Verde (22.935°W, 16.733°N). The western boundary in the VIIRS and MERRA-2 plots, panels (b), (d) and (f), is extended to 80°W, to highlight the propagation of the dust plume into the Caribbean and North America.

312 **3.2 Evaluation of the Dust Radiative Forcing**

313 Dust particles act to block the thermal radiation emitted by the Earth's surface, and scatter and
 314 absorb the SW radiation emitted by the Sun (Spyrou et al., 2018). These dust aerosol direct and
 315 semi-direct effects can be seen in Figs. 4a-b: the eastern tropical Atlantic, where the dust plume is
 316 located, exhibits higher surface net radiation fluxes, R_{net} , at night, when compared to the clearer
 317 regions further north around the Canary Islands ($\sim 0 \text{ W m}^{-2}$, as opposed to -100 W m^{-2}), and lower
 318 during the day ($\sim 500 \text{ W m}^{-2}$ compared to 800 W m^{-2} further north). The rather low values of R_{net}
 319 ($< 250 \text{ W m}^{-2}$) to the south of the plume and in parts of Mali are due the presence of deep convective
 320 clouds (Fig. 1c). The dust effects on R_{net} persisted for several days till the end of June 2020 (Fig.
 321 4c-d).

322



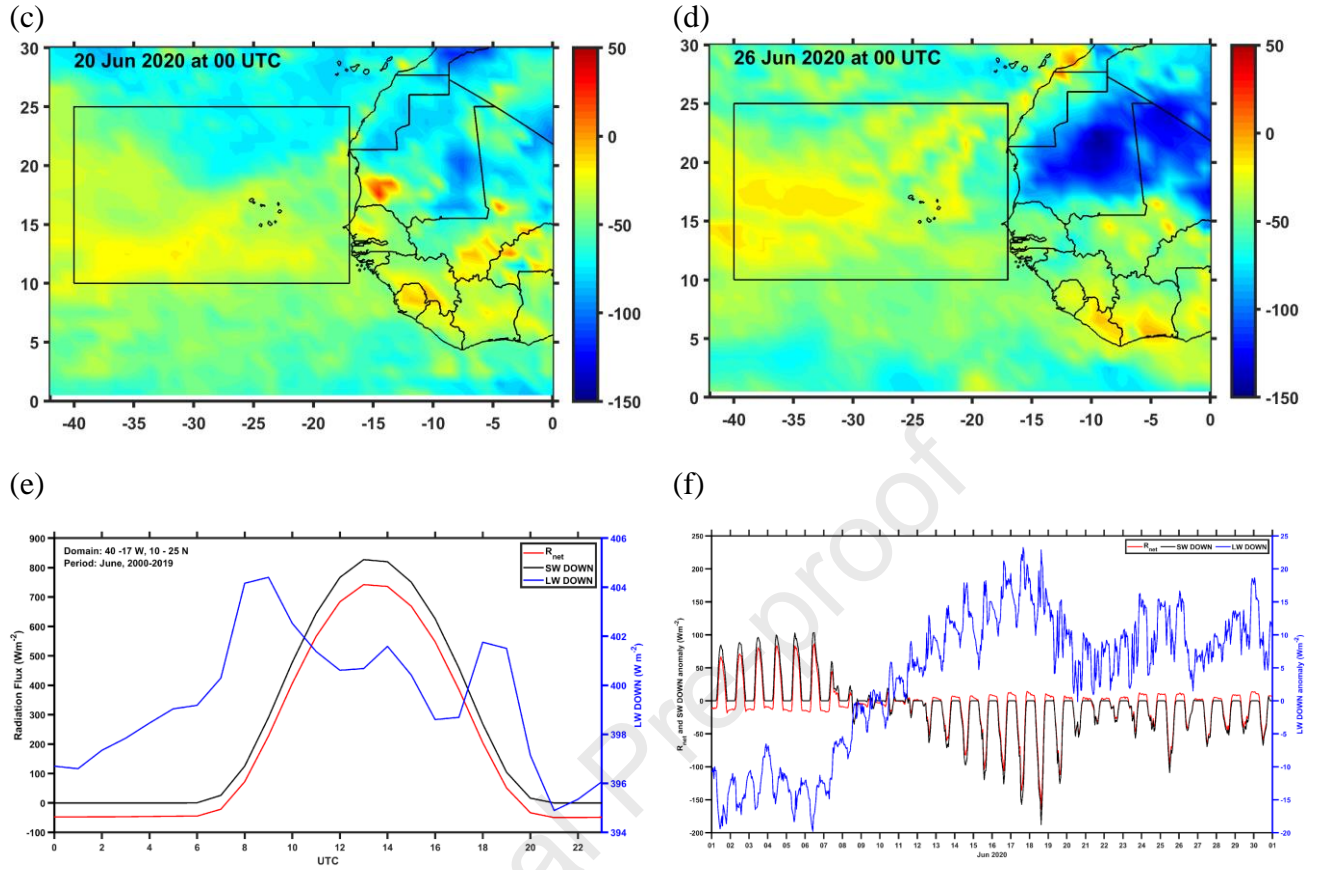


Figure 4. CERES net radiation flux at the surface, R_{net} ($W m^{-2}$), on 18 June 2020 at (a) 00 UTC and (b) 12 UTC; at 00 UTC on (c) 20 June 2020 and (d) 26 June 2020. (e) Climatological diurnal variation of area-averaged CERES downward short-wave and long-wave and R_{net} fluxes over the black rectangle in Fig. 1a. (f) is as (e) but showing the hourly anomalies for the month of June 2020.

323

324

325

326

327

328

329

330

331

332

333

334

335

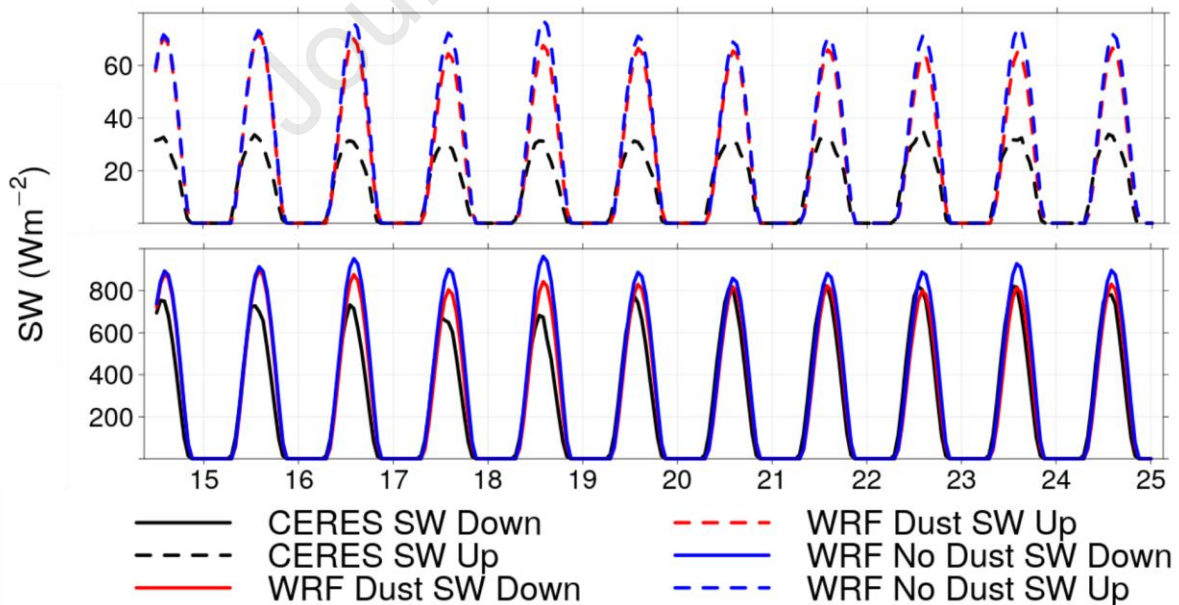
336

337

The DREs are also evident in the spatially-averaged time-series plots given in Figs. 4e-f. The R_{net} in the eastern tropical Atlantic typically varies between $-50 W m^{-2}$ at night and $+740 W m^{-2}$ during the day, largely following the diurnal cycle of the downward SW radiation flux. The daily maximum occurs at 13 UTC, when the 20-year standard deviation is roughly $40 W m^{-2}$, while the minimum takes place at 21 UTC, when the standard deviation is about $6 W m^{-2}$. However, during the June 2020 Saharan dust storm, R_{net} dropped by as much as $166 W m^{-2}$ during the day ($\sim 25\%$ of the mean value), with an anomaly of up to $+14 W m^{-2}$ at night ($\sim 28\%$ of the mean value). These numbers are roughly two to four standard deviations away from the mean, which underscores the extreme nature of this event. The nighttime increase in the downward LW radiation flux is also highly anomalous: the largest value of $\sim 23 W m^{-2}$ is about three standard deviations away from the mean. The reduction in the SW (up to $\sim 190 W m^{-2}$) and increase in the LW fluxes are up to three times larger than that modelled by Myhre et al. (2003) in the September 2000 Saharan dust storm, respectively. The former is also twice as large as that reported by Kaskaoutis et al. (2019) for a major dust storm in Greece, when the AOD exceeded 4.

338 The DRE from WRF can be estimated from the simulations with and without dust, given by the
 339 red and blue curves in Fig. 5, respectively. The maximum reduction in downward SW is $\sim 100 \text{ W m}^{-2}$
 340 m^{-2} while the increase in downward LW reaches up to $+20 \text{ W m}^{-2}$. These magnitudes are
 341 comparable to those modelled by Saidou Chaibou et al. (2020) over West Africa, by Haywood et
 342 al. (2003) and Highwood et al. (2003) off the coast of Africa, and are in line with those estimated
 343 by Anton et al. (2014), who studied a dust storm that affected southeastern Spain, for the predicted
 344 range of AODs. The modelled DREs for this event are larger than those estimated by Gutleben et
 345 al. (2020) for a dust event in the Caribbean, but smaller than those computed for the extreme
 346 September 2015 dust event over the eastern Mediterranean and the Middle East (Uzan et al., 2018),
 347 and for a major dust storm in Greece in March 2018 by Kaskaoutis et al. (2019). It is interesting
 348 to note that in the run without the dust feedback, the downward SW shows a day-to-day variability
 349 that has a comparable magnitude to the DRE, with a decrease of up to $\sim 100 \text{ W m}^{-2}$ from 16-17 and
 350 18-19 June, and an increase from 17 to 18 June due to the presence of clouds in the target region.
 351 A comparison with the CERES fluxes shows that WRF has a considerable bias: the model
 352 overestimates the downward SW by as much as 200 W m^{-2} , while the downward and upward LW
 353 fluxes are up to 20 W m^{-2} and 10 W m^{-2} smaller in WRF, respectively. When comparing the WRF
 354 simulation without dust and CERES (Figs. 4e-f and 5), the $\sim 200 \text{ W m}^{-2}$ difference in downward
 355 SW and $\sim 40 \text{ W m}^{-2}$ in downward LW are indicative of the net effect of dust, and are in line with
 356 the values obtained from the climatology analysis (Fig. 4f).
 357

(a)



(b)

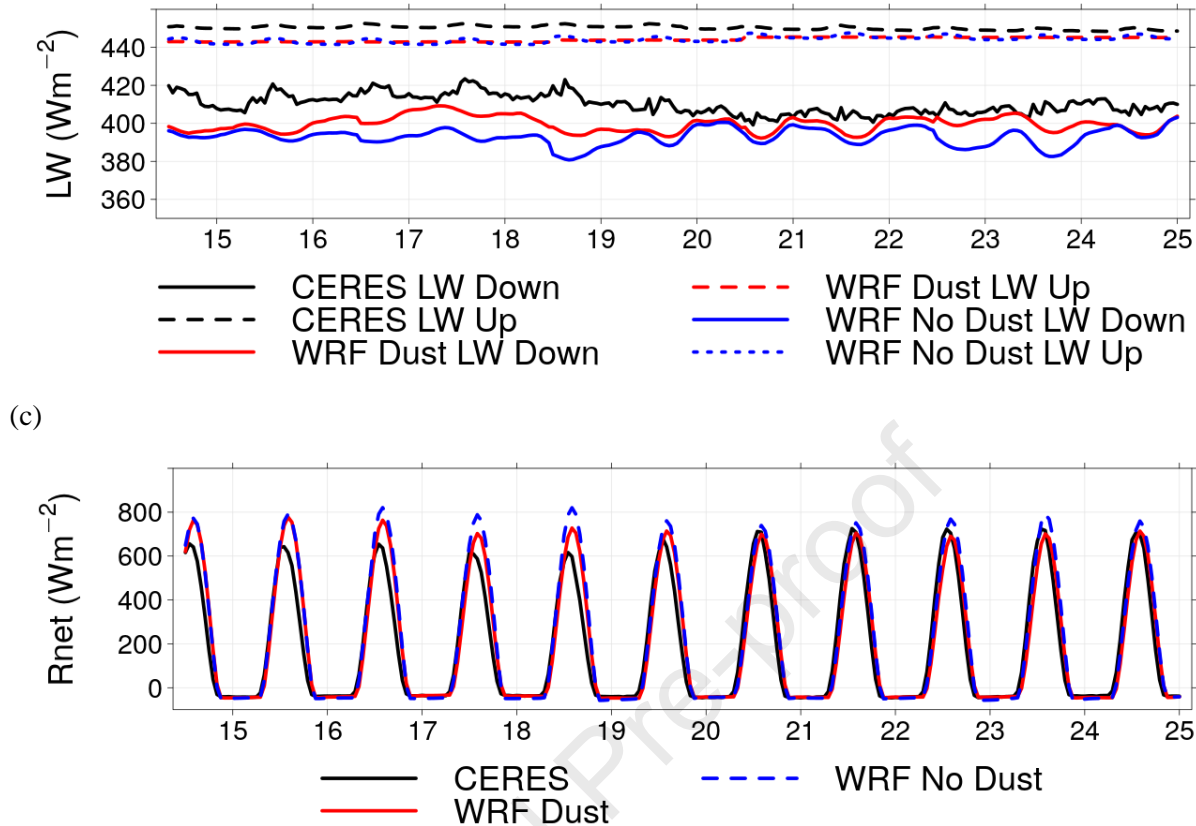


Figure 5. Time series of the upward (dashed line) and downward (solid line) (a) shortwave and (b) longwave radiative fluxes, and (c) net radiative flux (R_{net} ; $W m^{-2}$) from WRF (red) and CERES (black) averaged over $38^{\circ}W-17^{\circ}W$ & $10^{\circ}N-25^{\circ}N$ and for the period 14-24 June 2020. The predictions of the WRF simulations in which the DRE is accounted for are given by red lines, and those of the run without DRE are plotted in blue lines.

358

359 It is interesting to note that the dust effects on the upward SW radiation flux are much smaller than
 360 those on the downward SW radiation flux, mostly below $70 W m^{-2}$. This can be attributed to the
 361 low albedo of the sea surface (~ 0.06 ; e.g., Payne, 1972), which absorbs the vast majority of the
 362 incoming SW radiation. Similarly, the $\sim 20 W m^{-2}$ increase in the downward LW radiation flux is
 363 in contrast with a $< 5 W m^{-2}$ increase in the upward LW radiation flux. The latter is essentially
 364 controlled by the surface temperature, which exhibits a reduced variability over water as opposed
 365 to land regions due to its higher thermal inertia (e.g., Kawai and Wada, 2007).

366

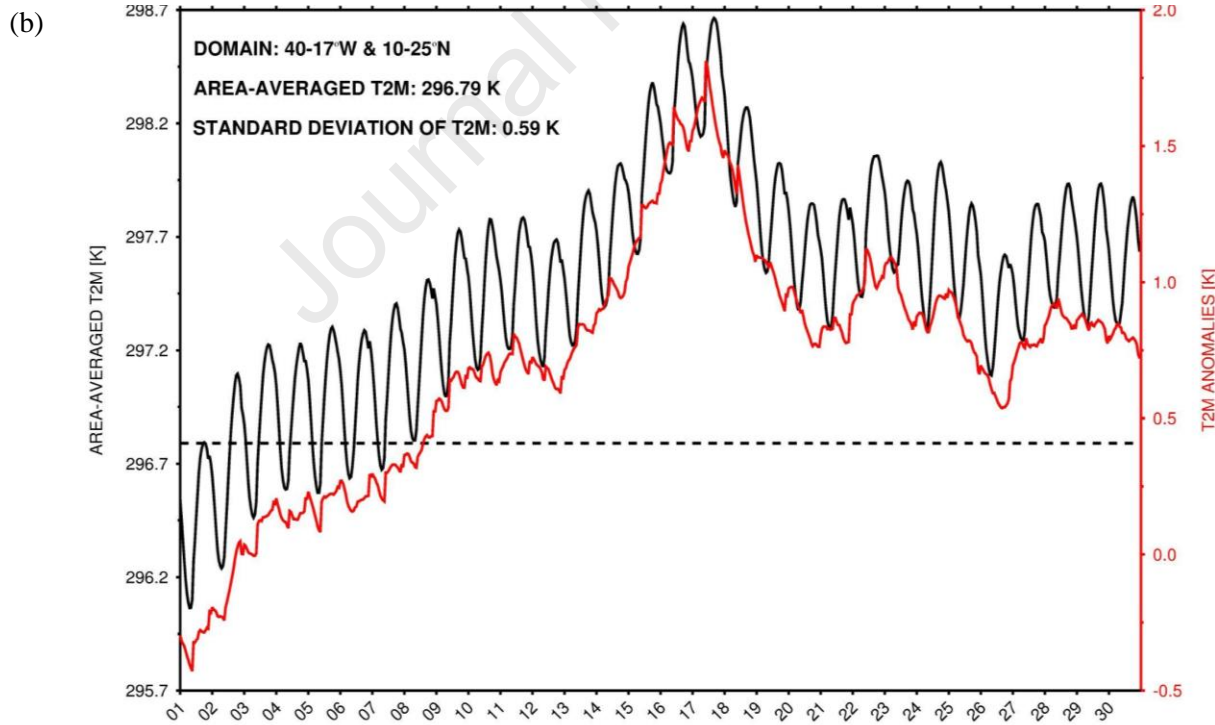
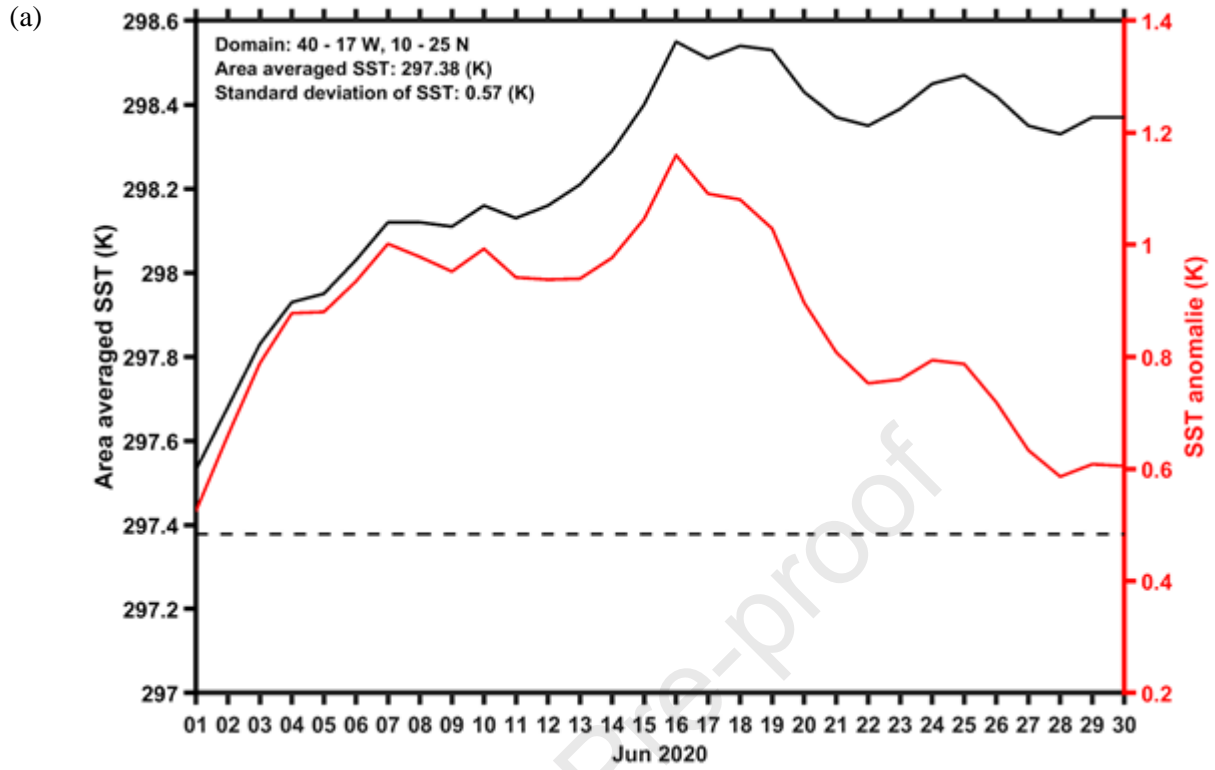
367 The radiative impact of dust on the sea surface and air temperature can be seen in Fig. 6, with Fig.
 368 6a giving the satellite-derived SSTs and Fig. 6b the air temperature from ERA-5. The SSTs,
 369 averaged over the eastern tropical Atlantic Ocean, increased by roughly 0.6-1.1 K during the event,
 370 a magnitude up to two times that of the climatological standard deviation. The air temperature rose
 371 by over 1.8 K, or about three times the climatological standard deviation. While the amplitude of
 372 the SST change is comparable to that reported by other studies over the eastern tropical Atlantic
 373 during Sahara dust outbreaks (e.g., Martinez Avellaneda et al., 2010; Jordan et al., 2018), the sign

374 is the opposite. The SST warming is likely due to the extremely high AODs observed in June 2020,
375 for which the heating of the ocean surface by the increased downward LW throughout the day
376 outweighs the cooling due to the reduced downward SW. In fact, the peak in SST anomalies on
377 24-25 June (Fig. 6a) takes place just after the AOD peak on 23 June (Fig. 2a). The warming of the
378 SSTs is consistent with the R_{net} and total energy flux F_{net} (given by R_{net} plus the heat fluxes) time-
379 series given in Figs. 6c and d, respectively. F_{net} remains relatively high from 15 to 18 June, with
380 anomalies as large as one third of its climatological standard deviation (Fig. 6d). This is an
381 indication of the heating of the surface. In fact, the maximum in SST (Fig. 6a) and 2-meter
382 temperature (Fig. 6b) occurs when the total energy flux at the surface is positive.

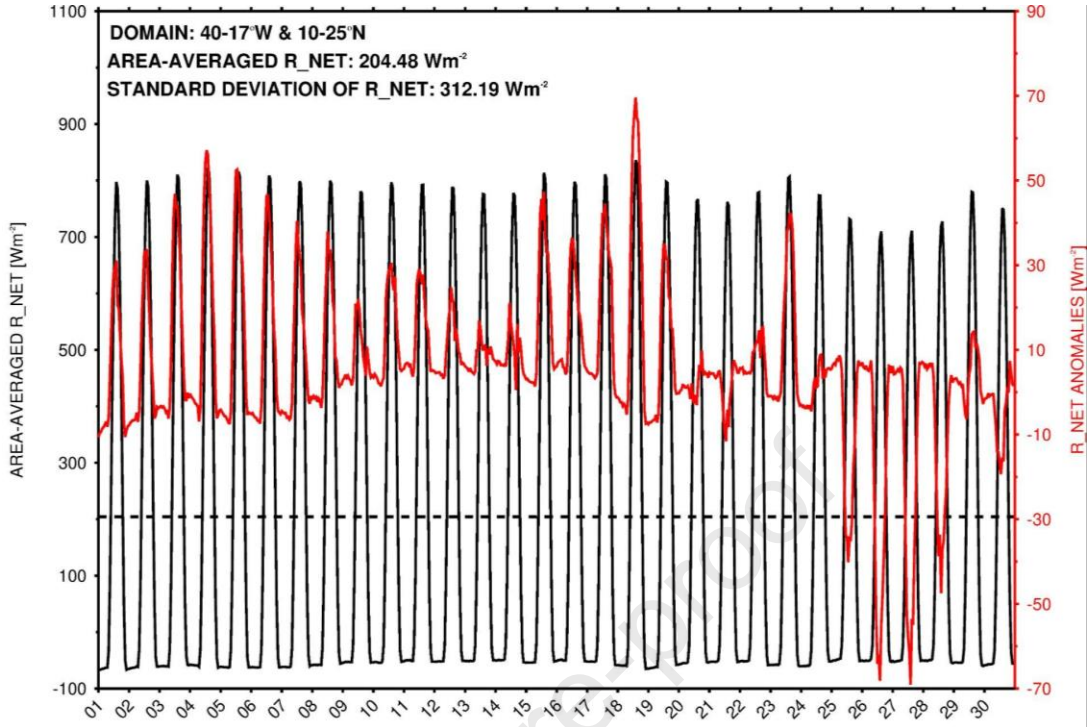
383 The dust aerosols' induced warming over the ocean is contradicting with the findings of previous
384 studies on the dust radiative impact. These studies were mainly based on modelling techniques and
385 concluded that the dust direct effect can increase the surface temperature over higher albedo
386 surface and decrease the surface temperature over lower albedo areas (Xie et al., 2018; Miller
387 2012; Takemura et al., 2009). However, when considering the dust radiative impact in the
388 longwave and by looking at daytime and nighttime observations separately (daily averaging leads
389 to the cancellation of daytime and nighttime effects), the results are different as evidenced in the
390 current study. Additionally, most of the current atmospheric models miss most of the large dust
391 particles in their simulated atmospheres and tend to deposit these particles too quickly near dust
392 source regions (Adebiyi and Kok, 2020) which leads to an underestimation of the dust radiative
393 impact in the longwave and hence in the net effect. Our results resonate with the findings of a new
394 study (Xian et al., 2020) in which the authors revisited the relationship between tropical cyclones
395 and dust aerosols and found a weak correlation between high dust aerosols and low tropical
396 cyclones activity over the tropical Atlantic Ocean. Should the nighttime/daytime dust effects have
397 been considered separately, the results by Xian et al., (2020) may have been further showing the
398 warming effect of dust aerosols at the surface.

399 The fact that an extremely dusty environment may lead to higher SSTs can be seen in Fig. 7, which
400 shows SEVIRI RGB and satellite-derived SST anomaly maps on 15, 18 and 23 June 2021. In these
401 figures, dustier regions are co-located with areas of positive SST anomalies exhibiting above-
402 average SSTs in places in excess of 4 K. It is important to note, when analyzing these results, that
403 due to the higher thermal inertia of water, it takes some time for the SSTs to respond to the
404 atmospheric forcing. Finally, it is interesting to note that the R_{net} anomalies from ERA-5, Fig. 6c,
405 are substantially different from those of CERES, Fig. 4f, in particular between 12 and 20 June.
406 This is an indication that the biases in the reanalysis dataset can still be considerable, despite the
407 extensive data assimilation employed.

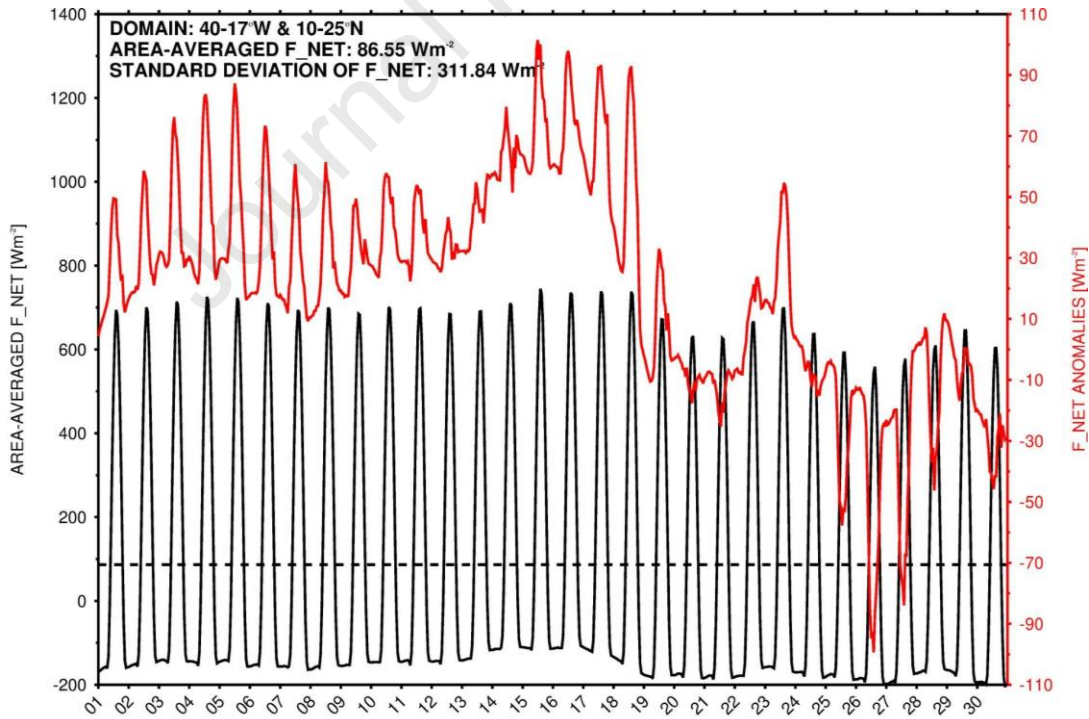
408



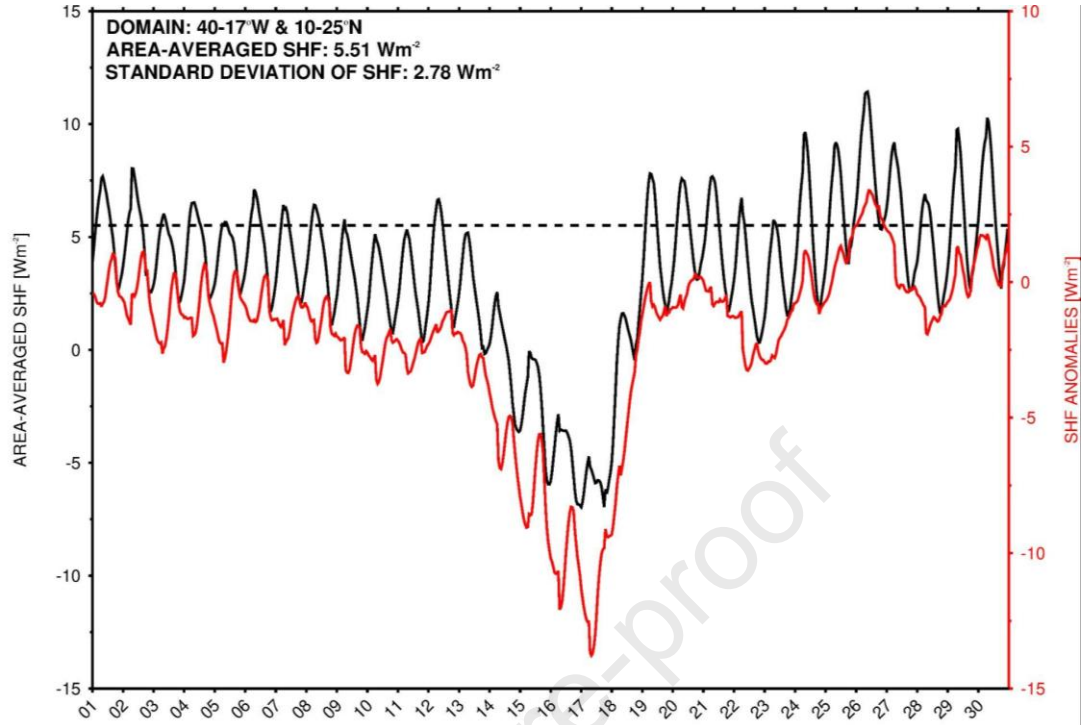
(c)



(d)



(e)



(f)

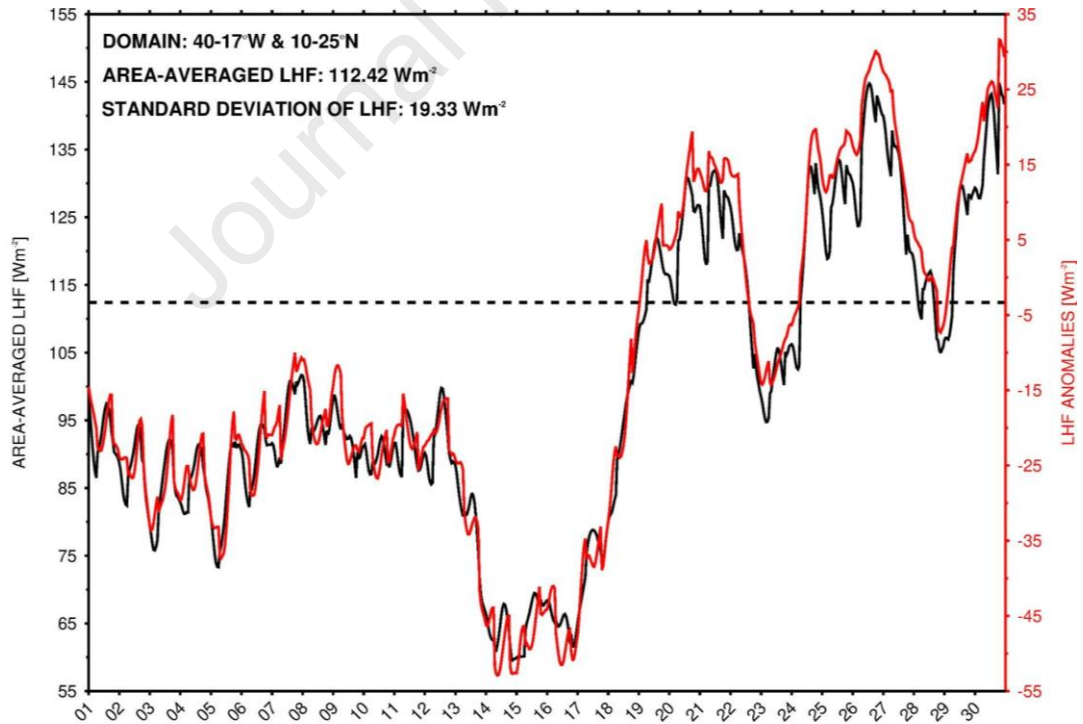
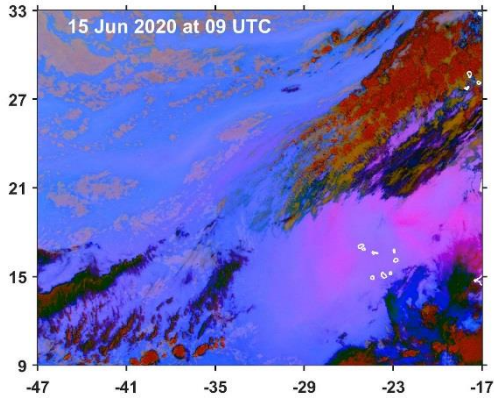


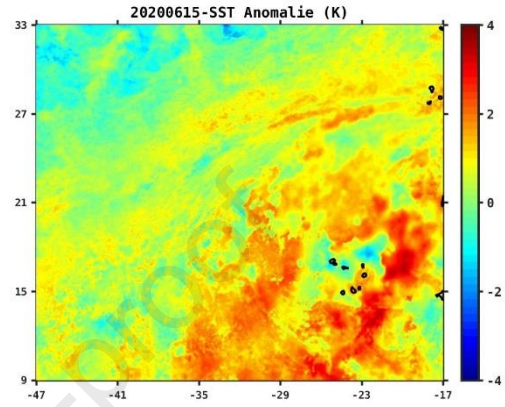
Figure 6. Averaged over 40-17°W & 10-25°N (black rectangle in Fig. 1) for the June 2020 actual values and anomalies of (a) Daily SSTs (K) from GHRSSST, and ERA-5 (b) 2-meter temperature (K), (c) total radiation flux (R_{net}), (d) total energy flux (F_{net}) at the surface in W m^{-2} (both positive if downward into

the surface), (e) sensible heat flux (SHF) and (f) latent heat flux (LHF) in W m^{-2} (both positive if upwards into the atmosphere). The GHRSSST anomalies are computed with respect to the 2002-2019 climatology, while those of ERA-5 are with respect to the 2000-2019 climatology, as GHRSSST data is not available prior to 2002. In all panels, the climatological mean and standard deviation are given at the top left, with the former also plotted as a dashed line.

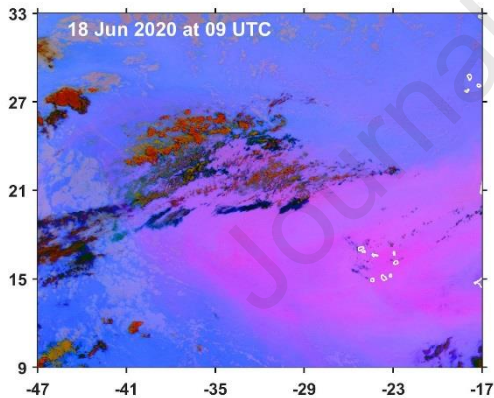
(a)



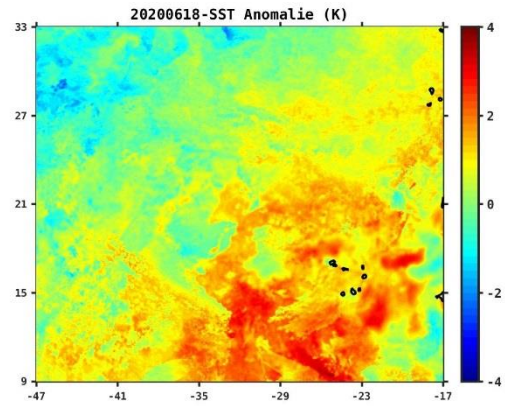
(b)



(c)



(d)



(e)

(f)

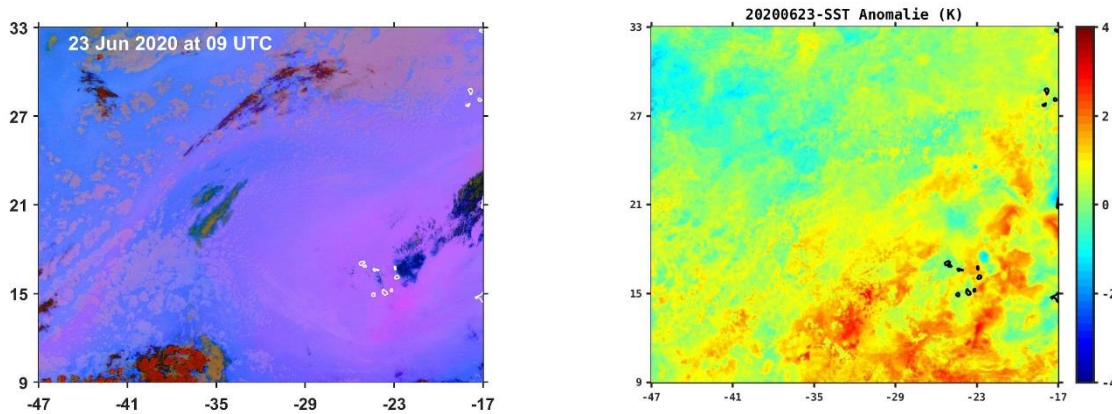


Figure 7: SEVIRI dust RGB snapshot at 09 UTC on (a) 15 June, (c) 18 June and (e) 23 June 2021. Thick high-level clouds are shaded in orange or brown; thin high-level clouds appear very dark (nearly black); dust is given in magenta or pink; sandy regions are highlighted in white; dry land is shaded in pale green. (b), (d) and (f) are GHRSSST anomalies with respect to the 2002-2019 climatology on the same days. All fields are shown for the domain 47°W-17°W and 9°N-33°N.

409 As far as the heat fluxes are concerned (Figs. 6e and 6f), the SHF and LHF drop by up to 14 and
 410 54 W m^{-2} , respectively, higher than the respective standard deviations. The variations of the SHF
 411 and LHF estimated for this event are roughly one half and four times larger than those modelled
 412 by Saidou Chaibou et al. (2020) over West Africa, respectively. The larger magnitude-change in
 413 the LHF compared to the SHF is in line with the fact that the target region in Saidou Chaibou et
 414 al. (2020) is over the desert, whereas here the fluxes are averaged over the ocean. The negative
 415 SHF is consistent with a warmer air temperature compared to the SSTs (i.e. downward pointing
 416 fluxes). Once the atmosphere becomes clearer, the surface-to-air temperature gradient decreases
 417 (Figs. 6a-b), which leads to a decrease in the SHF (i.e. it is less negative) and an increase in the
 418 LHF (enhanced surface evaporation). The warming of the surface seen here has important
 419 implications for the genesis and intensification of tropical storms: while the presence of a drier and
 420 dustier environment inhibits the formation of tropical disturbances (e.g., Reed et al., 2019), warmer
 421 SSTs and the resultant warming and moistening of the boundary layer have the opposite effect
 422 (e.g., Emanuel, 2005). As the dust plume extended all over the Atlantic Ocean (Fig. 3d and 3f),
 423 mostly near its primary breeding region just off the coast of Africa (Haggard et al., 1958), it is
 424 possible that the unprecedented June 2020 Saharan dust storm played a role in what was the most
 425 active Atlantic hurricane season on record, in particular in its early and rapid onset (Blackwell,
 426 2020).

427 **4. Conclusions**

428 In this study, the dust loading and radiative forcing for the June 2020 Saharan dust storm are
 429 estimated using a combination of observational and modelling products.

430

431 On 18 June, during the peak of the event, AOD estimates from satellite reached ~5, with the
432 MERRA-2 reanalysis and WRF underestimating it by up to one index unit. The dust loading over
433 the eastern tropical Atlantic is estimated at 7.9 Tg, a similar magnitude to that calculated over land
434 during previous major dust storms in the Sahara Desert (Bou Karam et al. 2009, 2010, 2014). A
435 comparable dust loading was observed in the following days, underscoring the persistent nature of
436 the emissions during this event.

437
438 The spatially-averaged reduction over the eastern tropical Atlantic Ocean in the downward SW
439 radiation flux reached $\sim 190 \text{ W m}^{-2}$ on 18 June, with an increase in the downward LW radiation by
440 up to 23 W m^{-2} , both larger than those observed at a single station in other major dust storms (e.g.,
441 Myhre et al., 2003; Kaskaoutis et al., 2019). As opposed to other events, however, there was an
442 increase in SSTs by as much as +1.1 K, and in the air temperature by up +1.8 K. This arises due to
443 a net warming of the surface, with an anomaly in the total energy flux of up to $\sim 100 \text{ W m}^{-2}$, roughly
444 a third of its climatological standard deviation. A comparison of the dust plume with the SSTs,
445 both estimated from satellite data, further suggests that heavy dust loadings may lead to higher
446 SSTs.

447
448 Over the last few decades, dust outbreaks from the Sahara Desert have been thought to induce
449 a net cooling at the surface and therefore contribute to the decrease in tropical storm activity over
450 the tropical Atlantic (e.g., Evan et al., 2006). However, our results show that the June 2020
451 historical dust storm induced a net warming over a sustained period of time. This is in line with
452 the findings of recent studies (Xian et al., 2020), which showed that the warming effect of dust
453 aerosols is larger than previously thought (e.g., Adebisi and Kok, 2020; Francis et al., 2020a).

454
455 These findings stress the importance of representing the radiative effects of dust aerosols in
456 general circulation models (GCMs) as well as in weather and climate models, in particular those
457 dedicated to the study and forecast of tropical storms and hurricanes. For example, the 2020
458 Atlantic hurricane season was record-breaking and was off to a fast start in May-July (Blackwell,
459 2020). Given that the Saharan dust reached all the way to North America, the aforementioned
460 increase in SSTs may have promoted the more active storm season, in particular as the largest SST
461 increases were around the breeding region for the so-called Cape Verde hurricanes, which are
462 typically the strongest of the season (Haggard, 1958). More investigation is needed in future
463 studies in order to disentangle the complex interconnection between the dust radiative forcing and
464 storm development and intensity. In particular, numerical experiments can be conducted to explore
465 the sensitivity of the SST response to varying levels of dust loading. Previous studies on the dust
466 radiative impact using GCMs have shown that the dust direct effect can increase the surface
467 temperature over higher albedo surface and decrease the surface temperature over lower albedo
468 areas (Xie et al., 2018; Miller 2012; Takemura et al., 2009). The findings of the current study do
469 not support those conclusions and invite the scientific community to investigate more carefully the
470 dust radiative impact in the longwave especially during night, and recommend a better

471 representation in GCMs of dust aerosols' size distribution (where large size particles are currently
472 underrepresented) and optical properties.

473

474 **Acknowledgments**

475 We wish to acknowledge the contribution of Khalifa University's high-performance computing
476 and research computing facilities to the results of this research. The SEVIRI satellite images were
477 downloaded from The European Organisation for the Exploitation of Meteorological Satellites
478 website (<https://eoportal.eumetsat.int/>). On the National Oceanic and Atmospheric Organization's
479 website, VIIRS (https://www.star.nesdis.noaa.gov/smcd/emb/viirs_aerosol/products.php),
480 CERES (<https://ceres.larc.nasa.gov/data/>) and GHRSSST (<http://ghrsst.nodc.noaa.gov>) data are
481 available, while MODIS (<https://modis.gsfc.nasa.gov/data/>) and AERONET
482 (<https://aeronet.gsfc.nasa.gov/>) data can be downloaded on the National Aeronautics and Space
483 Administration's website. All the data used in the present analysis are available here
484 <https://zenodo.org/record/4572733#.YKYoQqgzY2x>.

485

486 **Conflict of Interest:** The authors declare they don't have any conflict of interest.

487

488

489 **References**

- 490
491 Adebisi A. A., J. F. Kok, (2020), Climate models miss most of the coarse dust in the atmosphere. *Science*
492 *Advances*, 6, eaaz9507, doi: 10.1126/sciadv.aaz9507.
- 493
494 Al-Hemoud, A., Al-Sudairawi, M., Neelamanai, S., Naseeb, A. and Behbehani, W. (2017), Socioeconomic
495 effect of dust storms in Kuwait. *Arabic Journal of Geosciences*, 10(18), 1-9, doi: 10.1007/s12517-016-
496 2816.
- 497
498 Alpert, P. and Ganor, E. (1998), Sahara mineral dust measurements from TOMS: comparison to surface
499 observations over the Middle East for the extreme dust storm, March 14-17, 1998. *Journal of Geophysical*
500 *Research*, 106, 18275-18286, doi: 10.1029/2000JD900366.
- 501
502 Anton, M., Valenzuela, A., Mateos, D., Alados, I., Foyo-Moreno, I., Olmo, F. J. and Alados-Arboledas, L.
503 (2014), Longwave aerosol radiative effects during an extreme desert dust event in southeastern Spain.
504 *Atmospheric Research*, 149, 18-23, doi: 10.1016/j.atmosres.2014.05.022.
- 505
506 Azua-Bustos, A., Gonzalez-Silva, C., Fernandez-Martinez, M. A., Arenas-Fajardo, C., Fonseca, R., Martin-
507 Torres, F. J., Fernandez-Sampedro, M., Fairen, A. G. and Zorzano, M.-P. (2019), Aeolian transport of viable
508 microbial life across the Atacama Desert, Chile: Implications for Mars. *Scientific Reports*, 9, 11024, doi:
509 10.1038/s41598-019-47394-z.
- 510
511 Balkanski, Y., Bonnet, R., Boucher, O., Checa-Garcia, R. and Servonnat, J. (2021), Dust Induced
512 Atmospheric Absorption Improves Tropical Precipitations in Climate Models. *Atmospheric Chemistry and*
513 *Physics Discussion*, Under Review, doi: 10.5194/acp-2021-12.
- 514
515 Barnard, J. C., Fast, J. D., Paredes-Miranda, G., Arnott, W. P. and Laskin, A. (2010), Technical Note:
516 Evaluation of the WRF-Chem Aerosol Chemical to Aerosol Optical Properties Module using data from the
517 MILAGRO campaign. *Atmospheric Chemistry and Physics*, 10, 7325-7340, doi: 10.5194/acp-10-7325-
518 2010.
- 519
520 Bellouin, N., Quaas, J., Grysperdt, E., Kinne, S., Stier, P., Watson-Parris, D., Boucher, O., Carslaw, K. S.,
521 Christensen, M., Daniau, A.-L., Dufresne, J.-L., Feingold, G., Fiedler, S., Forster, P., Gettelman, A.,
522 Haywood, J. M., Lohmann, U., Malavelle, F., Mauritsen, T., McCoy, D. T., Myhre, G., Mulmenstadt, J.,
523 Neubauer, D., Possner, A., Rugenstein, M., Sato, Y., Schulz, M., Schwartz, S. E., Sourdeval, O., Storelvmo,
524 T., Toll, V., Winker, D. and Stevens, B. (2020), Bounding Global Aerosol Radiative Forcing of Climate
525 Change. *Reviews of Geophysics*, 58, e2019RG000660, doi: 10.1029/2019RG000660.
- 526
527 Blackwell, J. (2020), Record-breaking Atlantic hurricane season draws to an end. National Oceanic and
528 Atmospheric Administration, available online at [https://www.noaa.gov/media-release/record-breaking-](https://www.noaa.gov/media-release/record-breaking-atlantic-hurricane-season-draws-to-end)
529 [atlantic-hurricane-season-draws-to-end](https://www.noaa.gov/media-release/record-breaking-atlantic-hurricane-season-draws-to-end).
- 530

- 531 Bou Karam, D., Flamant, C., Cuesta, J., Pelon, J. and Williams, E. (2010), Dust emission and transport
532 associated with a Sharan depression: February 2007 case. *Journal of Geophysical Research*, 115, D00H27,
533 doi: 10.1029/2009JD012390.
- 534
535 Bou Karam, D., Flamant, C., Tulet, P., Chaboureau, J.-P., Dabas, A. and Todd, M. C. (2009), Estimate of
536 Sahelian dust emissions in the intertropical discontinuity region of the West African Monsoon. *Journal of*
537 *Geophysical Research*, 114, D13106, doi: 10.1029/2008JD011444.
- 538
539 Bou Karam, D., Williams, E., Janiga, M., Flamant, C., McGraw-Herdeg, M., Cuesta, J., Auby, A. and
540 Thorncroft, C. (2014), Synoptic-scale dust emissions over the Sahara Desert initiated by a moist convective
541 cold pool in early August 2006. *Quarterly Journal of the Royal Meteorological Society*, 140, 2591-2607,
542 doi: 10.1007/qj.2326.
- 543
544 Buchard, V., Randles, C. A., da Silva, A. M., Darmenov, A., Colarco, P. R., Govindaraju, R., Ferrare, R.,
545 Hair, J., Beyersdorf, A. J., Ziemba, L. D. and Yu, H. (2017), The MERRA-2 Aerosol Reanalysis, 1980
546 Onward. Part II: Evaluation and Case Studies. *Journal of Climate*, 30, 6851-6872, doi: 10.1175/JCLI-D-
547 16-0613.1.
- 548
549 Chen, D., Liu, Z., Davis, C. and Gu, Y. (2017), Dust radiative effects on atmospheric thermodynamics and
550 tropical cyclogenesis over the Atlantic Ocean using WRF-Chem coupled with an AOD data assimilation
551 system. *Atmospheric Chemistry and Physics*, 17, 7917-7939, doi: 10.5194/acp-17-7917-2017.
- 552
553 Chu, D. A., Kaufman, Y. J., Ichoku, C., Remer, L. A., Tanre, D. and Holben, B. N. (2002), Validation of
554 MODIS aerosol optical depth retrieval over land. *Geophysical Research Letters*, 29(12), doi:
555 10.1029/2001GL013205.
- 556
557 Choobari, A., Zawar-Reza, P. and Sturman, A. (2014), The global distribution of mineral dust and its
558 impacts on the climate system: A review. *Atmospheric Research*, 138, 152-165, doi:
559 10.1016/j.atmosres.2013.11.007.
- 560
561 Colarco, P. R., Toon, O. B. and Holben, B. N. (2003), Saharan dust transport to the Caribbean during
562 PRIDE: 1. Influence of dust sources and removal mechanisms on the timing and magnitude of downwind
563 aerosol optical depth events from simulations of in situ and remote sensing observations. *Journal of*
564 *Geophysical Research: Atmospheres*, 108, 8589, doi: 10.1029/2002JD002658.
- 565
566 Di Bagio, C., Formenti, P., Balkanski, Y., Caponi, L., Cazaunau, M., Pangui, E., Journet, E., Nowak, S.,
567 Caqueneau, S., Andrae, O. M., Kandler, K., Saeed, T., Piketh, S., Seibert, D., Williams, E., Doussin, J. F.
568 C. (2017), Global scale variability of the mineral dust long-wave refractive index: A new dataset of in situ
569 measurements for climate modeling and remote sensing. *Atmospheric Chemistry and Physics*, 17, 1901-
570 1929, doi: 10.5194/acp-17-1901-2017.
- 571
572 Doelling, D. R., Loeb, N. G., Keyes, D. F., Nordeen, M. L., Morstad, D., Nguyen, C., Wielicki, B. A.,
573 Young, D. F. and Sun, M. (2013), Geostationary Enhanced Temporal Interpolation for CERES Flux

- 574 Products. *Journal of Atmospheric and Oceanic Technology*, 30, 1072-1090, doi: 10.1175/JTECH-D-12-
575 00136.1
- 576
- 577 Doelling, D. R., Sun, Nguyen, L. T., Nordeen, M. L., Haney, C. O., Keyes, D. F. and Mlynyczak, P. E.
578 (2016), Advances in Geostationary-Derived Longwave Fluxes for the CERES Synoptic (SYN1deg)
579 Product. *Journal of Atmospheric and Oceanic Technology*, 33, 503-521, doi: 10.1175/JTECH-D-15-
580 0147.1.
- 581
- 582 Dubovik O., A. Sinyuk, T. Lapyonok, B.N. Holben, M. Mishchenko, P. Yang, T.F. Eck, H. Volten, O.
583 Muñoz, B. Veihelmann, W.J. van der Zande, J.-F. Leon, M. Sorokin, I. Slutsker, Application of spheroid
584 models to account for aerosol particle non sphericity in remote sensing of desert dust *J. Geophys. Res.*, 111
585 (2006), p. D11208, 10.1029/2005JD006619
- 586
- 587 Dy, C. Y. and Fung, J. C. H. (2016), Updated global soil map for the Weather Research and Forecasting
588 model and soil moisture initialization for the Noah land surface model. *Journal of Geophysical Research*,
589 121, 8777-8800, doi: 10.1002/2015JD024558.
- 590
- 591 Eltahan, M., Shokr, M. and Sherif, A. O. (2018), Simulation of Severe Dust Events over Egypt Using Tuned
592 Dust Schemes in Weather Research Forecast (WRF-Chem). *Atmosphere*, 9, 246, doi:
593 10.3390/atmos9070246.
- 594
- 595 Emanuel, K. (2005), Increasing destructiveness of tropical cyclones over the past 30 years. *Nature*, 436,
596 686-688, doi: 10.1038/nature03906.
- 597
- 598 Evan, A. T., Dunion, J., Foley, J. A., Heidinger, A. K., and Velden, C. S. (2006), New evidence for a
599 relationship between Atlantic tropical cyclone activity and African dust outbreaks, *Geophys. Res. Lett.*, 33,
600 L19813, doi:10.1029/2006GL026408.
- 601
- 602 Evan, A. T., Foltz, G. R. and Zhang, D. (2012), Physical Response of the Tropical-Subtropical North
603 Atlantic Ocean to Decadal-Multidecadal Forcing by African Dust. *Journal of Climate*, 25, 5817-5829, doi:
604 10.1175/JCLI-D-11-00438.1.
- 605
- 606 Evan, A. T., Foltz, G. R., Zhang, D. and Vimont, D. J. (2011), Influence of African dust on ocean-
607 atmosphere variability in the tropical Atlantic. *Nature Geosciences*, 4, 762-765, doi: 10.1038/ngeo1276.
- 608
- 609 Flaounas, E., Kotroni, V., Lagouvardos, K., Klose, M., Flamant, C. and Giannaros, T. M. (2017), Sensitivity
610 of the WRF-Chem (V3.6.1) model to different dust emission parametrisation: assessment in the broader
611 Mediterranean region. *Geoscientific Model Development*, 10, 2925-2945, doi: 10.5194/gmd-10-2925-
612 2017.
- 613
- 614 Francis, D., Alshamsi, N., Cuesta, J., Isik, A. G. and Dundar, C. (2019), Cyclogenesis and Density Currents
615 in the Middle East and the Associated Dust Activity in September 2015. *Geosciences*, 9(9), 376, doi:
616 10.3390/geosciences9090376.
- 617

- 618 Francis, D. Chaboureau, J.-P., Nelli, N., Cuesta, J., Al Shamsi, N., Temimi, M., Pauluis, O. and Xue, L.
619 (2020a), Summertime dust storms over the Arabian Peninsula and impacts on radiation, circulation, cloud
620 development and rain. *Atmospheric Research*, 250, 105364, doi: 10.1016/j.atmosres.2020.105364.
621
- 622 Francis, D., Fonseca, R., Nelli, N., Cuesta, J., Weston, M., Evan, A. and Temimi, M. (2020b), The
623 atmospheric drivers of the major Saharan dust storm in June 2020. *Geophysical Research Letters*, 47,
624 e2020GL090102, doi: 10.1029/2020GL090102.
625
- 626 Gelato, R., McCarty, W., Suarez, M. J., Todling, R., Molod, A., Takacs, L., Randles, C. A., Darmenov, A.,
627 Bosilovich, M. G., Reichle, R., Wargan, K., Coy, L., Cullather, R., Draper, C., Akella, S., Buchard, V.,
628 Conaty, A., da Silva, A. M., Gu, W., Kim, G.-K., Koster, R., Lucchesi, R., Merkova, D., Nielsen, J. E.,
629 Partyka, G., Pawson, S., Putman, W., Rienecker, M., Schubert, S. D., Sienkiewicz, M. and Zhao, B. (2017),
630 The Modern-Era Retrospective Analysis for Research and Applications, version 2 (MERRA-2). *Journal of*
631 *Climate*, 30, 5419-5454, doi: 10.1175/JCLI-D-16-0758.1.
632
- 633 Ginnadaki, D., Pizzer, A. and Lelieveld, J. (2014), Modeled global effects of airborne desert dust on air
634 quality and premature mortality. *Atmospheric Chemistry and Physics*, 14, 957-968, doi: 10.5194/acp-14-
635 957-2014.
636
- 637 Ginoux, P., Chin, M., Tegen, I., Goddard, T. and In, G. (2001), Sources and distributions of dust aerosols
638 simulated with the GOCART model. *Journal of Geophysical Research: Atmospheres*, 106, 20255-20273,
639 doi: 10.1029/2000JD000053.
640
- 641
- 642 Grell, G. A. and Dvnyi, D. (2002), A generalized approach to parameterizing convection combining
643 ensemble and data assimilation techniques. *Geophysical Research Letters*, 29, 10-13, doi:
644 10.1029/2002GL015311.
645
- 646 Grell, G. A., Peckham, S. E., Schmitz, R., McKeen, S. A., Frost, G., Skamarock, W. C. and Eder, B. (2005),
647 Fully coupled “online” chemistry with the WRF model. *Atmospheric Environment*, 39, 6957-6975, doi:
648 10.1016/j.atmosenv.2005.04.027.
649
- 650 Griffin, D. W., Kellogg, C. A., Garrison, V. H and Shinn, E. A. (2002), The Global Transport of Dust: An
651 Intercontinental river of dust, microorganisms and toxic chemical flows through the Earth’s atmosphere.
652 *American Scientist*, 90(3), 228-235, doi: 10.1511/2002.3.228.
653
- 654 Gutleben, M., Grob, S., Wirth, M. and Mayer, B. (2020), Radiative effects of long-range-transported
655 Saharan air layers as determined from airborne lidar measurements. *Atmospheric Chemistry and Physics*,
656 20, 12313-12327, doi: 10.5194/acp-20-12313-2020.
657
- 658 Haggard, W. H. (1958), The Birthplace of North Atlantic Tropical Storms. *Monthly Weather Review*,
659 86(10), 397-404, doi: 10.1175/1520-0493(1958)086<0397:TBNAT>2.0.CO;2.
660

- 661 Hamzeh, N. H., Karami, S., Kaskaoutis, D. G., Tegen, I., Moradi, M. and Opp, C. (2021), Atmospheric
662 Dynamics and Numerical Simulations of Six Frontal Dust Storms in the Middle East Region. *Atmosphere*,
663 12, 125, doi: 10.3390/atmos12010125.
- 664
- 665 Haywood, J. and Boucher, O. (2000), Estimates of the direct and indirect radiative forcing due to
666 tropospheric aerosols: A review. *Reviews of Geophysics*, 38(4), 513–543, doi: 10.1029/1999RG000078.
- 667
- 668 Haywood J.M., R.P. Allan, I. Culverwell, T. Slingo, S. Milton, J. Edwards, N. Clerbaux
669 Can desert dust explain the outgoing longwave radiation anomaly over the Sahara during July 2003? *J.*
670 *Geophys. Res.*, 110 (2005), p. D05105, 10.1029/2004JD005232
- 671
- 672 Haywood, J. M., Francis, P., Osborne, S. R., Glew, M., Loeb, N., Highwood, E., Tanre, D., Myhre, G.,
673 Formenti, P. and Hirst, E. (2003), Radiative properties and direct radiative effect of Saharan dust measured
674 by the C-130 aircraft during SHADE: 1. Solar spectrum. *Journal of Geophysical Research*, 108(D18), 8577,
675 10.1029/2002JD002687.
- 676
- 677 Heald C.L., D.A. Ridley, J.H. Kroll, S.R.H. Barrett, K.E. Cady-Pereira, M.J. Alvarado, C.D. Holmes,
678 Contrasting the direct radiative effect and direct radiative forcing of aerosols, *Atmos. Chem. Phys.*, 14
679 (2014), pp. 5513-5527, 10.5194/acp-14-5513-2014.
- 680
- 681 Heinold B., I. Tegen, K. Schepanski, O. Hellmuth, Dust Radiative Feedback on Saharan Boundary Layer
682 Dynamics and Dust Mobilization *Geophys. Res. Lett.*, 35 (2008), p. L20817, 10.1029/2008GL035319.
- 683
- 684 Hersbach, H., Bell, B., Berrisford, P., Dahlgren, P., Horanyi, A., Muñoz-Sebater, J., Nicolas, J., Radu, R.,
685 Schepers, D., Simmons, A., Soci, C. (2020), The ERA5 Global Reanalysis: achieving a detailed record of
686 the climate and weather for the past 70 years. European Geophysical Union General Assembly 2020, May
687 3 - 8, Vienna, Austria, doi: 10.5194/egusphere-egu2020-10375.
- 688
- 689 Highwood, E. J., Haywood, J. M., Silverstone, M. D., Newman, S. M. and Taylor, J. P. (2003), Radiative
690 properties and direct effect of Saharan dust measured by the C-130 aircraft during SHADE. 2: Terrestrial
691 spectrum. *Journal of Geophysical Research*, 108(D18), 8578, 10.1029/2002JD002552.
- 692
- 693 Holben, B. N., Eck, T. F., Slutsker, I., Tanre, D., Buis, J. P., Setzer, A., Vermote, E., Reagan, J. A.,
694 Kaufman, Y. J., Nakajima, T., Lavenu, F., Jankowiak, I. and Smirnov, A. (1998), AERONET - A Federated
695 Instrument Network and Data Archive for Aerosol Characterization. *Remote Sensing of the Environment*,
696 66, 1-16, doi: 10.1016/s0034-4257(98)00031-5.
- 697
- 698 Hong, S. Y., Noh, Y. and Dudhia, J. (2006), A new vertical diffusion package with an explicit treatment of
699 entrainment processes. *Monthly Weather Review*, 134, 2318-2341, doi: 10.1175/MWR3199.1.
- 700
- 701 Iacono, M. J., Delamere, J. S., Mlawer, E. J., Shepherd, M. W., Clough, S. A. and Collins, W. D. (2008),
702 Radiative forcing by long-lived greenhouse gases: Calculations with the AER radiative transfer models.
703 *Journal of Geophysical Research*, 113, D13103, doi: 10.1029/2008JD009944.
- 704

- 705 Ito, A., Abediyi, A. A., Huang, Y. and Kok, J. F. (2021), Less atmospheric radiative heating due to
706 aspherical dust with coarser size. *Atmospheric Chemistry and Physics Discussion (Under Review)*, doi:
707 10.5194/acp-2021-134.
708
- 709 Jia R., Y. Liu, S. Hua, Q. Zhu, T. Shao, Estimation of the aerosol radiative effect over the Tibetan Plateau
710 based on the latest CALIPSO product, *J. Meteorol. Res.*, 32 (2018), pp. 707-722, 10.1007/s13351-018-
711 8060-3.
712
- 713 Jimenez, P. A., Dudhia, J., Gonzalez-Rouco, J. F., Navarro, J., Montvez, J. P. and Garcia-Bustamante, E.
714 (2012), A revised scheme for the WRF surface layer formulation. *Monthly Weather Review*, 140, 898-918,
715 doi: 10.1175/MWR-D-11-00056.1.
716
- 717 Jordan, A. K., Gnanadesikan, A. and Zaitchik, B., (2018), Simulated Dust Aerosol Impacts on Western
718 Sahelian Rainfall: Importance of Ocean Coupling. *Journal of Climate*, 31(22), 9107-9124, doi:
719 10.1175/JCLI-D-17-0819.1.
720
- 721 Kabatas, B., Pierce, R. B., Unal, A., Rogal, M. J. and Lenzen, A. (2018), April 2008 Saharan dust event:
722 Its contribution to PM10 concentrations over the Anatolian Peninsula and relation with synoptic conditions.
723 *Science of The Total Environment*, 533, 317-328, doi: 10.1016/j.scitotenv.2018.03.150.
724
- 725 Kaskaoutis, D. G., Dumka, U. C., Rashki, A., Psiloglou, B. E., Gavriil, A., Mofidi, A., Petrinoli, K.,
726 Karagiannis, D. and Kambezidis, H. D. (2019), Analysis of intense dust storms over the eastern
727 Mediterranean in March 2018: Impact on radiative forcing and Athens air quality. *Atmospheric*
728 *Environment*, 209, 23-39, doi: 10.1016/j.atmosenv.2019.04.025.
729
- 730 Kaufman, Y. J., Tanre, D., Rmer, L. A., Vermote, E. F., Chu, A. and Holben, B. N. (1997), Operational
731 remote sensing of tropospheric aerosol over land from EOS moderate resolution imaging spectroradiometer.
732 *Journal of Geophysical Research*, 102, 17501-17067, doi: 10.1029/96JD03988.
733
- 734 Kawai, Y. and Wada, A. (2007), Diurnal sea surface temperature variation and its impact on the atmosphere
735 and ocean: A review. *Journal of Oceanography*, 63, 721-744, doi: 10.1007/s10872-007-0063-0.
736
- 737 Kok, J. F., Adebisi, A. A., Albani, S., Balkanski, Y., Checa-Garcia, R., Chin, M., Colarco, P. R., Hamilton,
738 D. S., Huang, Y., Ito, A., Klose, M., Li, L., Mahowald, N. M., Miller, R. L., Obiso, V., Pérez García-Pando,
739 C., Rocha-Lima, A., and Wan, J. S.: Contribution of the world's main dust source regions to the global cycle
740 of desert dust, *Atmos. Chem. Phys.*, 21, 8169–8193, <https://doi.org/10.5194/acp-21-8169-2021>, 2021.
741
- 742 Kosmopoulos P.G., S. Kazadzis, M. Taylor, E. Athanasopoulou, O. Speyer, P.I. Raptis, E. Marinou, E.
743 Proestakis, S. Solomos, E. Gerasopoulos, V. Amiridis, A. Bais, C. Kontoes, Dust impact on surface solar
744 irradiance assessed with model simulations, satellite observations and ground-based measurements, *Atmos.*
745 *Meas. Tech.*, 10 (2017), pp. 2435-2453, 10.5194/amt10-2435-2017
746

- 747 Legrand, S. L., Polashenski, C., Letcher, T. W., Creighton, G. A., Peckham, E. and Cetola, J. D. (2018),
748 The AFWA Dust Emissions Scheme for the GOCART Aerosol Model in WRF-Chem. *Geoscientific Model*
749 *Development*, 12, 131-166, doi: 10.5194/gmd-12-131-2019.
- 750
751 Levy, R. and Hsu, C. (2015a), MODIS Atmosphere L2 Aerosol Product. NASA MODIS Adaptive
752 Processing System, Goddard Space Flight Center, USA, doi: 10.5067/MODIS/MOD04_L2.061.
- 753
754 Levy, R. and Hsu, C. (2015b), MODIS Atmosphere L2 Aerosol Product. NASA MODIS Adaptive
755 Processing System, Goddard Space Flight Center, USA, doi: 10.5067/MODIS/MYD04_L2.061.
- 756
757 Levy, R. C., Remer, L. A., Martins, J. V., Kaufman, Y. J., Plana-Fattori, A., Redemann, J. and Wenny, B.
758 (2005), Evaluation of the MODIS Aerosol Retrievals over Ocean and Land during CLAMS. *Journal of*
759 *Atmospheric Sciences*, 62(4), 974-992, doi: 10.1175/JAS3391.1.
- 760
761 Lin, Y. L., Farley, R. D. and Orville, H. D. (1983), Bulk parameterization of the snow field in a cloud
762 model. *Journal of Applied Meteorology and Climatology*, 22, 1065-1092, doi: 10.1175/1520-
763 0450(1983)022<1065:BPOTSF>2.0.CO;2.
- 764
765 Liu, L., Huang, X., Ding, A. and Fu, C. (2016), Dust-induced radiative feedbacks in north China: A dust
766 storm episode modeling study using WRF-Chem. *Atmospheric Environment*, 129, 43-54, doi:
767 10.1016/j.atmosenv.2016.01.019.
- 768
769 Loveland, T. R., Reed, B. C., Ohlen, D. O., Brown, J. F., Zhu, Z., Yang, L. and Merchant, J. W. (2000),
770 Development of a global land cover characteristics database and IGBP DISCover from 1 km AVHRR.
771 *International Journal of Remote Sensing*, 21, 1303-1330, doi: 10.1080/014311600210191.
- 772
773 Manktelow, P. T., Carslaw, K. S., Mann, G. W. and Spracklen, D. V. (2010), The impact of dust on sulfate
774 aerosol, CN and CCN during an East Asian dust storm. *Atmospheric Chemistry and Physics*, 10, 365-382,
775 doi: 10.5194/acp-10-365-2010.
- 776
777 Martin, M., Dash, P., Ignatov, A., Banzon, V., Beggs, H., Brasnett, B., Cavula, J.-F., Cummings, J., Donlon,
778 C., Gentemann, C., Grumbine, R., Ishizaki, S., Maturi, E., Reynolds, R. W. and Roberts-Jones, J. (2012),
779 Group for High Resolution Sea Surface Temperature (GHRSSST) analysis fields inter-comparisons. Part 1:
780 A GHRSSST multi-product ensemble (GMPE). *Deep Sea Research Part II: Topical Studies in*
781 *Oceanography*, 77-80, 21-30, doi: 10.1016/j.dsr2.2012.04.013.
- 782
783 Martinez, M. A., Ruiz, J. and Cuevas, E. (2009), Use of SEVIRI images and derived products in a WMO
784 Sand and dust Storm Warning System. *IOP Conference Series: Earth and Environmental Science*, 7,
785 012004, doi: 10.1088/1755-1307/7/1/012004.
- 786
787 Martinez Avellaneda, N. M., Serra, N., Minnett, P. J. and Stammer, D. (2010), Response of the eastern
788 subtropical Atlantic SST to Saharan dust: A modeling and observational study. *Journal of Geophysical*
789 *Research*, 115, C08015, doi: 10.1029/2009JC005692.
- 790

- 791 Miller, S. D., Straka III, W., Mills, S. P., Elvidge, C. D., Lee, T. F., Solbrig, J., Walther, A., Heidinger, A.
792 K. and Weiss, S. C. (2013), Illuminating the Capabilities of the Suomi National Polar-Orbiting Partnership
793 (NPP) Visible Infrared Imaging Radiometer Suite (VIIRS) Day/Night Band. *Remote Sensing*, 5, 6717-
794 6766, doi: 10.3390/rs5126717.
- 795
- 796 Miller, R. L. (2012). Adjustment to radiative forcing in a simple coupled ocean-atmosphere model. *Journal*
797 *of Climate*, 25, 7802-7821, <https://doi.org/10.1175/JCLI-D-11-00119.1>.
- 798
- 799 Myhre, G., Grini, A., Haywood, J. M., Stordal, F., Chatenet, B., Tanré, D., Sundet, J. K. and Isaksen, I. S.
800 A. (2003), Modeling the radiative impact of mineral dust during the Saharan Dust Experiment (SHADE)
801 campaign. *Journal of Geophysical Research*, 108, 8579, doi: 10.1029/2002JD002566.
- 802
- 803 NCEP (2015), NCEP GFS 0.25 Degree Global Forecast Grids Historical Archive.
- 804
- 805 Nelli, N. R., Temimi, M., Fonseca, R. M., Weston, M. J., Thota, M. S., Valappil, V. K., Branch, O.,
806 Wizemann, H.-D., Wulfmeyer, V. and Wehbe, Y. (2020) Micrometeorological measurements in an arid
807 environment: Diurnal characteristics and surface energy balance closure. *Atmospheric Research*, 234,
808 104745, doi: 10.1016/j.atmosres.2019.104745.
- 809
- 810 Payne, R. E. (1972), Albedo of the Sea Surface. *Journal of Atmospheric Sciences*, 29, 959-979, doi:
811 10.1175/1520-0469(1972)029<0959:AOTSS>2.0.CO;2.
- 812
- 813 Prakash P.J., G. Stenchkov, S. Kalenderski, S. Osipov, H. Bangalath, The impact of dust storms on the
814 Arabian Peninsula and the Red Sea, *Atmos. Chem. Phys.*, 15 (2015), pp. 199-222, 10.5194/acp-15-199-
815 2015.
- 816
- 817 Reed, K. A., Bacmeister, J. T., Huff, J. J. A., Wu, X., Bates, S. C. and Rosenbloom, N. A. (2019), Exploring
818 the impact of dust on North Atlantic hurricanes in a high-resolution climate model. *Geophysical Research*
819 *Letters*, 46, 1105-1112, doi: 10.1029/2018GL080642.
- 820
- 821 Remer, L. A., Kaufman, Y. J., Tanre, D., Mattoo, S., Chu, D. A., Martins, J. V., Li, R.-R., Ichoku, C., Levy,
822 R. C., Kleidman, R. G., Eck, T. F., Vermote, E. and Holben, B. N. (2005) The MODIS Aerosol Algorithm,
823 Products, and Validation. *Journal of Atmospheric Sciences*, 62(4), 947-973, doi: 10.1175/JAS3385.1.
- 824
- 825 Rodriguez-Cotto, R., Ortiz-Martinez, M. G., Rivera-Ramirez, E., Mendez, L. B., Davila, J. C. and Jimenez-
826 Velez, B. D. (2013), African Dust Storms Reaching Puerto Rican Coast Stimulate the Secretion of IL-6 and
827 IL-8 and Cause Cytotoxicity to Human Bronchial Epithelial Cells (BEAS-2B). *Health (Irvine Calif)*,
828 5(10B), 14-28, doi: 10.4236/health.2013.510A2003.
- 829
- 830 Rontu, L., Gleeson, E., Perez, D. M., Nielsen, K. P. and Toll, V. (2020), Sensitivity of Radiative Fluxes to
831 Aerosols in the ALADIN-HIRLAM Numerical Weather Prediction System. *Atmosphere*, 11(2), 205, doi:
832 10.3390/atmos11020205.
- 833

- 834 Saeed, T. M., Al-Dashti, H. and Spyrou, C. (2014), Aerosol's optical and physical characteristics and direct
835 radiative forcing during a shamal dust storm, a case study. *Atmospheric Chemistry and Physics*, 14, 3751-
836 3769, doi: 10.5194/acp-14-3751-2014.
- 837
- 838 Saleeby S.M., S.C. van den Heever, J. Bukowski, A.L. Walker, J.E. Solbrig, S.A. Atwood, Q. Bian, S.M.
839 Kreidenweis, Y. Wang, J. Wang, S.D. Miller, 'The influence of simulated surface dust lofting and
840 atmospheric loading on radiative forcing', *Atmos. Chem. Phys.*, 19 (2019), pp. 10279-10301, 10.5194/acp-
841 19-10279-2019.
- 842
- 843 Sanchez, P. A., Ahmed, S., Carre, F., Hartemink, A. E., Hempel, J., Huising, J., Lagacherie, P., McBratney,
844 A. B., McKenzie, N. J., Mendonca-Santos, M. L., Minasny, B., Montanarella, L., Okoth, P., Palm, C. A.,
845 Sachs, J. D., Shepherd, K. D., Vagen, T.-G., Vanlauwe, B., Walsh, M. G., Winowiecki, L. A. and Zhang,
846 G.-L. (2009), Digital soil map of the world. *Science*, 325, 680-681, doi: 10.1126/science.1175084.
- 847
- 848 Saidou Chaibou, A. A., Ma, X. and Sha, T. (2020), Dust radiative forcing and its impact on surface energy
849 budget over West Africa. *Scientific Reports*, 10, 12236, doi: 10.1038/s41598-020-69223-4.
- 850
- 851 Schmetz, J., Pili, P., Tjemkes, S., Just, D., Kerkmann, J., Rota, S. and Ratier, A. (2002), An introduction to
852 Meteosat Second Generation (MSG). *Bulletin of the American Meteorological Society*, 83, 977-992, doi:
853 10.1175/1520-0477(2002)083<0977:AITMSG.2.3.CO;2.
- 854
- 855 Sertel, E., Robock, A. and Ormeci, C. (2010), Impacts of land cover data quality on regional climate
856 simulations. *International Journal of Climatology*, 30, 1942-1953, doi: 10.1002/joc.2036.
- 857
- 858 Satheesh, S. K. and Krishna Moorthy, K. (2005), Radiative effects of natural aerosols: A review.
859 *Atmospheric Environment*, 39, 2089-2110. doi: 10.1016/j.atmosenv.2004.12.029.
- 860
- 861 Singh, C., Kumar Singh, S., Chauhan, P. and Budakoti, S. (2021), Simulation of an extreme dust episode
862 using WRF-CHEM based on optimal ensemble approach. *Atmospheric Research*, 249, 105296, doi:
863 10.1016/j.atmosres.2020.105296.
- 864
- 865 Skamarock, W. C., Klemp, J. B., Dudhia, J., Gill, D. O., Barker, D. M., Duda, M. G., Huang, X.-Y., Wang,
866 W. and Powers, J. G. (2008), A Description of the Advanced Research WRF Version 3. NCAR, doi:
867 10.5065/D68S4MVH.
- 868
- 869 Slingo, A., Ackerman, T. P., Allan, R. P., Kassianov, E. I., McFarlane, S. A., Robinson, G. J., Barnard, J.
870 C., Miller, M. A., Harries, J. E., Russell, J. E. and Dewitte, S. (2006), Observations of the impact of a major
871 Saharan dust storm on the atmospheric radiation balance. *Geophysics Research Letters*, 33, L24817, doi:
872 10.1029/2006GL027869.
- 873
- 874 Sokolik, I. N., Winker, D. M., Bergametti, G., Gillette, D. A., Carmichael, G., Kaufman, Y. J., Gomes, L.,
875 Schuetz, L. and Penner, J. E. (2001), Introduction to special section: Outstanding problems in quantifying
876 the radiative impacts of mineral dust. *Journal of Geophysical Research*, 106, 18015-18027, doi:
877 10.1029/2000JD900498.

- 878
879 Solomos, S., Ansmann, A., Mamouri, R.-E., Biniotoglou, I., Patlakas, P., Marinou, E. and Amiridis, V.
880 (2017), Remote sensing and modelling analysis of the extreme dust storm hitting the Middle East and
881 eastern Mediterranean in September 2015. *Atmospheric Chemistry and Physics*, 17, 4063-4078, doi:
882 10.5194/acp-17-4063-2017.
- 883
884 Solomos, S., Kalivitis, N., Mihalopoulos, N., Amiridis, V., Kouvaris, G., Gkikas, A., Biniotoglou, I.,
885 Tsekeri, A., Kazadzis, S., Kottas, M., Pradhan, Y., Proestakis, E., Nastos, P. T. and Marengo, F. (2018),
886 From Tropospheric Folding to Khamsin and Foehn Winds: How Atmospheric Dynamics Advanced a
887 Record-Breaking Dust Episode in Crete. *Atmosphere*, 9, 240, doi: 10.3390/atmos9070240.
- 888
889 Su, L. and Fung, J. C. H. (2015), Sensitivities of WRF- Chem to dust emission schemes and land surface
890 properties in simulating dust cycles during springtime over East Asia. *Journal of Geophysical Research*
891 *Atmosphere*, 120, 11215– 11230, doi: 10.1002/2015JD023446.
- 892
893 Spyrou, C. (2018), Direct radiative impacts of desert dust on atmospheric water content. *Aerosol Science*
894 *and Technology*, 52, 693-701, doi: 10.1080/02786826.2018.1449940.
- 895
896 Spyrou, C., Kallos, G., Mitsakou, C., Athanasiadis, P., Kalogeri, C. and Iacono, M. J. (2013), Modeling the
897 radiative effects of desert dust on weather and regional climate. *Atmospheric Chemistry and Physics*, 13,
898 5489-5504, doi: 10.5194/acp-13-5489-2013.
- 899
900 Takemura, T., Egashira, M., Matsuzawa, K., Ichijo, H., O'ishi, R., & Abe-Ouchi, A. (2009). A simulation
901 of the global distribution and radiative forcing of soil dust aerosols at the Last Glacial Maximum.
902 *Atmospheric Chemistry and Physics*, 9, 3061-3073. <https://doi.org/10.5194/acp-9-3061-2009>.
- 903
904 Tanre, D., Haywood, J. M., Pelon, J., Leon, J. F., Chatenet, B., Formenti, P., Francis, P., Goloub, P.,
905 Highwood, E. J. and Myhre, G. (2003), Measurement and modeling of the Saharan dust radiative impact:
906 overview of the SaHArAn Dust Experiment (SHADE). *Journal of Geophysical Research*, 8574, 108(D13),
907 10.1029/2003JD003273.
- 908
909 Teixeira, J. C., Carvalho, A. C., Tuccella, P., Curci, G. and Rocha, A. (2016), WRF-Chem sensitivity to
910 vertical resolution during a saharan dust event. *Physics and Chemistry of the Earth, Parts A/B/C*, 94, 188-
911 195, doi: 10.1016/j.pce.2015.04.002.
- 912
913 Tewari, M., Chen, F., Wang, W., Dudhia, J., Lemone, M. A., Mitchell, K., Ek, M., Gayno, G., Wegiel, J.
914 and Cuenca, R. H. (2004), Implementation and verification of the unified NOAA land surface model in the
915 WRF model. 20th conference on weather analysis and forecasting / 16th conference on numerical weather
916 prediction, 11-15, available online at <https://ams.confex.com/ams/pdfpapers/69061.pdf>.
- 917
918 Todd, M. C., Bou Karam, D., Cavazos, C., Bouet, C., Heinold, B., Baldasano, J. M., Cautenet, G., Koren,
919 I., Perez, C., Solomon, F., Tegen, I., Tulet, P., Washington, R. and Zakey, A. (2008), Quantifying
920 uncertainty in estimates of mineral dust flux: An intercomparison of model performance over the Bodele
921 Depression, northern Chad. *Journal of Geophysical Research*, 113, D24107, doi: 10.1029/2008JD010476.

- 922
923 Uzan, L., Egert, S. and Alpert, P. (2018), New insights into the vertical structure of the September 2015
924 dust storm employing eight ceilometers and auxiliary measurements over Israel. *Atmospheric Chemistry
925 and Physics*, 18, 3203-3221, doi: 10.5194/acp-18-3203-2018.
926
- 927 Wang J., U. Nair, S.A. Christopher (2004) GOES-8 Aerosol optical thickness assimilation in a mesoscale
928 model: Online integration of aerosol radiative effects, *J. Geophys. Res.*, 109 (2004),
929 10.1029/2004JD004827D23203.
930
- 931 Wang, H., Shi, G., Li, S., Li, W., Wang, B. and Huang, Y. (2006), The impacts of optical properties on
932 radiative forcing due to dust aerosol. *Advances in Atmospheric Sciences*, 23, 431-441, doi:
933 10.1007/s00376-006-0431-5.
934
- 935 Wang W., J. Huang, T. Zhou, J. Bi, L. Lin, Y. Chen, Z. Huang, J. Su (2013) Estimation of radiative effect
936 of a heavy dust storm over Northwest China using Fu–Liou model and ground measurements, *Elsevier J.
937 Quant. Spectr. Radiat. Transf.*, 122 (2013), pp. 114-126, 10.1016/j.jqsrt.2012.10.018.
938
- 939 Wang, Y., Chen, L., Xin, J. and Wang, X. (2020), Impact of the Dust Aerosol Model on the VIIRS Aerosol
940 Optical Depth (AOD) Product across China. *Remote Sensing*, 12, 991, doi: 10.3390/rs12060991.
941
- 942 Wang, W., Mao, F., Pan, Z., Du, L. and Gong, W. (2017), Validation of VIIRS AOD through a Comparison
943 with a Sun Photometer and MODIS AODs over Wuhan. *Remote Sensing*, 9, 403, doi: 10.3390/rs9050403.
944
- 945 Weston, M. J., M. Temimi, N. R. Nelli, R. M. Fonseca, M. S. Thota and V. K. Valappil (2020), On the
946 Analysis of the Low-Level Double Temperature Inversion Over the United Arab Emirates: A Case Study
947 during April 2019, *IEEE Geoscience and Remote Sensing Letters*, 1-5, doi: 10.1109/LGRS.2020.2972597.
948
- 949 Xie, X., Liu, X., Che, H., Xie, X., Wang, H., Li, J., ... Liu, Y. (2018). Modeling East Asian dust and its
950 radiative feedbacks in CAM4-BAM. *Journal of Geophysical Research: Atmospheres*, 123, 1079-1096.
951 <https://doi.org/10.1002/2017JD027343>.
952
- 953 Zeng, X. and Beljaars, A. (2005), A prognostic scheme of sea surface skin temperature for modeling and
954 data assimilation. *Geophysical Research Letters*, 32, L14605, doi: 10.1029/2005GL023030.
955
- 956 Zhao, C., Liu, X., Ruby Leung, L. and Hagos, S. (2011), Radiative impact of mineral dust on monsoon
957 precipitation variability over West Africa. *Atmospheric Chemistry and Physics*, 11, 1879-1893, doi:
958 10.5194/acp-11-1879-2011.

The Radiative Impact of the June 2020 historical Saharan Dust Storm

Diana Francis^{1*}, Narendra Nelli¹, Ricardo Fonseca¹, Michael Weston¹, Cyrille Flamant², Charfeddine Cherif¹

¹ Environmental and Geophysical Sciences Lab, Khalifa University, P.O. Box 127788, Abu Dhabi, UAE.

² CNRS and UVSQ, LATMOS, Sorbonne Universités, 75005 Paris, France.

Corresponding Author: diana.francis@ku.ac.ae

Conflict of Interest: The authors declare they don't have any conflict of interest.